Characterization and impact on reservoir quality of fractures in the Cretaceous Qamchuqa Formation, Zagros folded belt

Rashid, F.[1], Hussein, D.[2], Lawrence, J.A.[3], Khanaqa[4], P.

[1] Kurdistan institution for strategic study and scientific research, Sulaimani, Iraq. Email: fraidoon.rashid@kissr.edu.krd, Phone: +9647701924416

[2] Geology Department, University of Sulaimani, Sulaimani, Iraq.

[3] Department of Civil and Environmental Engineering, Imperial College London, UK.

Abstract

Reservoir quality in fractured carbonate rocks is controlled by the fracture properties, the tectonic origin of fractures, the relationship of fractures to other sedimentary features within the rockmass and diagenesis. In this study fracture analysis, porosity and permeability of the Qamchuqa Formation in Miran West block from the Zagros folded belt in Kurdistan has been studied using core analysis, micro-resistivity image logs, drill stem tests (DST), mud logging data, Repeat Formation Test (RFT), drilled cutting samples and wireline log data.

The integrated analysis showed that the Qamchuqa Formation is characterized by heterogeneous sedimentary and tectonic features including burial stylolites, dissolution seams, tectonic stylolites, cemented veins, open fractures and partially open mineralized fractures. The sedimentary features include burial stylolites, dissolution seams and some fractures which formed at early stages of burial and diagenesis (Phase 1), while open fractures, partially open mineralized fractures, veins and tectonic stylolites were formed by later tectonic activity (Phase 2). It was found that the fracture properties including aperture, length, frequency and origin all play an important role in controlling the reservoir quality. Structures including stylolites, dissolution seams and veins had a general negative impact on reservoir quality by occlusion of pore spaces and blocking the fluid flow of the original rock

matrix. In contrast, the open and partially open mineralized fractures enhanced the rock pore connectivity and provide well inter-connected fracture networks and consequently provided very high fracture permeability.

Keywords. Fracture; porosity; permeability; carbonate reservoir; Qamchuqa Formation.

1 Introduction

Carbonate reservoir rocks often store huge accumulations of hydrocarbons within their heterogeneous microstructures and naturally occurring fractures (Aydin, 2000; Cooper, 2007; Garland et al., 2010; Al-Qayim and Rashid, 2012; Al-Qayim and Othman, 2012; Lamarche et al., 2012; Lavenu et al., 2014; Zebari and Burberry, 2015). The reservoir quality is usually defined in terms of pore connectivity and permeability. Petrophysical properties of the rocks (original and diagenetic modifications) and fracture distribution have major impacts on reservoir quality in carbonate rocks. Fractures in carbonate rocks provide enhanced pore connectivity and provide well connected fluid flow pathways through different types of reservoirs which is especially important in tight, heterogeneous carbonate rocks (Neuzil and Tracy, 1981; Laubach, 2003; Barr, 2007; Agosta etal., 2010; Solano etal., 2011; Korneva etal., 2014; Rashid et al., 2015a; Rashid et al., 2015b; Rashid et al., 2017; Dashti et al., 2018).

Carbonates are often considered to have dual permeability with fluid flow through the matrix and the fractures. The fracture network may dominate increasing storage, permeability and direction of hydrocarbon flow (Huntoon and Lundy, 1979). Fractures may cut individual beds or several beds and they can have extreme effects increasing the magnitude of permeability in carbonate reservoirs (Singh et al., 2009).

Understanding the role of fractures in enhancing reservoir quality is complex and relies on predicting fracture network distribution, then extrapolating and calculating how this contributes to exploration risk. Natural fractures can increase borehole instability and decrease the reservoir pressure as the fracture spaces close after a period of production (Nelson, 2001). In addition, non-hydrocarbon fluids may pass through the fractures dissolving the rock matrix or filling the fracture pores with secondary minerals, consequently reducing the reservoir porosity and permeability (Barker et al., 2006; Dietrich et al., 1983). Understanding fracture networks, their geological history and diagenetic evolution is considered crucial when evaluating and optimizating carbonate reservoir rocks and for production planning (Becker et al, 2018). Thus, investigations of fracture network morphologies have been used as a tool to better characterize the reservoir and improve drilling operations and production management (Narr, 1996; Peacock et al., 2003; Wennberg et al., 2006; Gillespie et al., 2011; Wilson et al., 2011; Lamarche et al., 2012; Zeeb et al., 2013; Peacock et al., 2018).

The Zagros Basin is characterized by a complex sub-surface structural region, where multiple oil and gas fields have been discovered (Beydoun et al., 1992; Cooper, 2007). A series of fracture studies have been undertaken in the Iranian Zagros region including McQuillan (1973) and (1974); Nemati and Pezeshk, (2006); Wennberg et al., (2006); Navabpour et al., (2007); Stephenson et al., (2007); Ahmadhadi et al., (2008); Rajabi et al., (2010); Casini et al., (2011); Lacombe et al., (2011); Lapponi et al., (2011); Tavani et al., (2011); Navabpour et al., (2012); Carminati et al., (2013); Pireh et al., (2015); Joudaki et al., (2016); Casini et al., (2018); Dashti et al, (2018); Tavani et al., (2018) but far fewer studies have been undertaken in the Iraqi region of the Zagros Basin (north and north western Iraq), examples include Garland et al, (2010); Csontos et al, (2012); Garland et al, (2012); Reif et al., (2012) ; Awdal et al., (2013); Zebari, (2013); Zebari and Burberry, (2015); and Awdal et al, (2016). Investigations of fracture origin and timing can be challenging in carbonate reservoir rocks. Fracture orientation, length, spacing and aperture (opening) all govern fracture permeability (Miranda et al., 2018). These factors are considered as a function of position within the folds, rock microstructure and beds thickness within the Zagros region (Wenberg et al., 2006).

This work describes the fracture distribution and characteristics of the Lower Cretaceous, Qamchuqa Formation which is a carbonate reservoir in Zagros fold belt. The study area is situated along the north-eastern part of the Iraqi Zagros Basin which is poorly characterised due to a limited exploration and fracture investigations. The data was collected from the Miran West field and compared static data with dynamic data including mud logging data and test results in order to understand the fracture influence on production potential and to support future field development planning. In addition, subsurface core samples and micro-resistivity borehole imaging data sets have been collated and used as an analogue to better understand the reservoir fracture properties. The objective of this research is to investigate the paragenesis of fracture formation in heterogeneous carbonate rocks and the influence of fracturing on the reservoir quality.

2 Geologic setting

Two wells drilled in the Miran West field (Figure 1) were chosen for this study, MW-1 exploration well and MW-2 appraisal well. MW-2 included a cored section of the Qamchuqa Formation from 1066 m to 1187 m. These wells penetrate the Cretaceous, Aptian to Middle Turonian Stage, Qamchuqa Formation which is a carbonate hydrocarbon bearing rock and a reservoir target. The region investigated is the Miran West structure within the Zagros Fold Belt in the Kurdistan Region of north-eastern Iraq where the majority of hydrocarbon production comes from carbonate reservoirs (Motiei, 1993; Alavi, 2007). The Miran structure is a thrusted anticlinal fold with a northwest to southeast oriented axis with fault closure to the northwest and southeast. The structure is about 70 km long and 15 km wide, some 12 km west of the city of Sulaimani (Figure 1). The Miran structure trends parallel to the other structures of the Zagros folded belt that covers about 2000 km starting in south-eastern Turkey and continuing through Northern Iraq into southern Iran (Versfelt, 2001).

The structure is located close to the northern boundary of the NW-SE trending Kirkuk Embayment region of the Zagros Fold and Thrust Belt. The Zagros Mountains formed during Cretaceous and Tertiary collision of the Arabia and Eurasia plates (Talbot and Alavi, 1996; Fakhari and Soleimany, 2003; Homke et al., 2004; Sherkati and Letouzey, 2004; Fard et al., 2006; Homke et al., 2009; Khadivi et al., 2010; Saura et al., 2011; Koshnaw et al., 2018). The Zagros deformation zone is characterised by strike-slip and contractional movements. These movements result from strain being partitioned into dextral strike-slip movements along mainly NW-SE faults and a shortening component in a NE-SW direction (Vernant et al., 2004).

Relatively tight, high relief anticlinal structures have been observed on seismic images which are considered to be heavily faulted, fractured and deformed rocks (Heritage, 2010). The folding and faulting have influenced the density, frequency and development of the fracture distribution throughout the stratigraphic succession (Heritage, 2009 and 2010).

The tectonic evolution during the early Cretaceous was defined by the cessation of westward motion of the Arabian Plate, as a result of the opening of the South Atlantic Ocean (Iranpanah and Esfandiari, 1979). The motion of the central Iranian plates also ceased in response to the closure of the Palaeo-Tethys Ocean (Sattarzadeh et al., 2000). Thus, the relative motion of the Arabian and Central Iranian Plates reversed and north-eastward subduction of the Neo-Tethyan crust under the Iranian plates was initiated. This interval was characterised by a moderately high, but falling, eustatic sea level (Haq et al., 1988). The eastern shelf platform of the Arabian Plate including the current Zagros folded belt was covered by shallow marine water, on a passive margin depositing the Qamchuqa Formation carbonates. A series of inner-facies were identified as evaporates and siliciclastics of the Jawan Formation in the eastern part of the Kirkuk embayment and subsequently passed into deeper water limestone of the Balambo Formation to the east of the Kirkuk embayment and further into northeast Iraq (Buday, 1980; Numan, 1983; Jassim and Goff, 2005; Aqrawi et al., 2010; Al-Qayim and Rashid, 2012).

In the region four formations are exposed at surface ranging from Palaeocene to Eocene age; these are the Kolosh Formation (Upper Palaeocene), Sinjar Formation (Lower Eocene), Gercus Formation (Middle Eocene), and PilaSpi (Upper Eocene). The Kolosh and Sinjar formations dominate most of the area whereas the other formations form a narrow strip along the western part of the greater Miran structure (Figure 1). Three common regional carbonate reservoirs of the Cretaceous petroleum system (Qamchuqa, Kometan and Shiranish) are present in the sub-surface of the structure (Jassim and Goff, 2005; Aqrawi et al., 2010). These formations have different reservoir qualities and petrophysical properties. However, the reservoir zones are bound by relative mechanical strength of the rock intervals rather than stratigraphic boundaries. In addition four unconventional reservoir zones have been identified at the Miran West Structure two within the Jurassic (Zones 1 and 2) and two in the Cretaceous (Zones 3 and 4) (Heritage, 2009 and 2010).

3 Materials and Methodologies

The fracture analysis was performed in the Qamchuqa Formation interval of wells MW-1 and MW-2 drilled in the Miran West Field. The core section of Well MW-2 was drilled entirely in the Qamchuqa Formation and achieved 98% core recovery. Plug samples were drilled from the cores to measure the gas porosity and permeability. Furthermore, the cores, cutting samples and wireline log data have been used to develop a detailed stratigraphic column of the Qamchuqa Formation in the study area (Figure 2). A summary of the gathered data in this study are presented in Table (1).

The Miran West-1 (MW-1) well was the first exploration well drilled by Heritage Energy Middle East Ltd in the Kurdistan Region of Iraq (Heritage, 2009). The well was drilled as a vertical exploration wildcat at the crest of the Miran West structure was targeting multiple reservoir intervals including Cretaceous, Jurassic and Triassic rocks. The well was vertical through the Tertiary and Cretaceous intervals, but a slight inclination to built 4.1° in the top of Jurassic Formations and reached 5.6° by TD.

The Miran West-2 (MW-2) well was the second well drilled by Heritage Energy Middle East Ltd in the Kurdistan Region of Iraq (Heritage, 2009). It was drilled initially as a vertical well on the Miran West structure and is located about 6 km northwest of the MW-1. This well targeted multiple reservoirs in the Cretaceous and Jurassic. The well path maintained an almost vertical profile in the Tertiary and Cretaceous intervals. The highest well inclination recorded was 7.1° at the top of Jurassic successions and this deviation reduced to 3.4° at TD.

A detailed rock description and stratigraphic study was conducted based on core observations, microscopic study of cutting samples, combined with well logs. The drilled cutting samples were used for lithologic description for the non-cored intervals in well MW-2 and all intervals of the Qamchuqa Formation in well MW-1. Lithologic variation and stratigraphic study of the Qamchuqa Formation were achieved from rock samples supported by lithological and mineralogical investigation obtained from the wireline log data (GR, DT, LDS, and CNL). Dunhams (1962) classification was used to identify the carbonate microfacies. The rock descriptions were used to interpret and describe sedimentary texture, microstructures, lithology, colour, microfacies, sedimentary structure, diagenesis and tectonic effects, thickness variation was measured manually (Wang et al., 2015; Al-Qayim and Rashid, 2012; Honarmand and Amini, 2012).

To characterize the Qamchuqa Formations matrix porosity and permeability a set of cylindrical plug samples (6 cm to 6.5 cm in length and 3.8 cm in diameter) were drilled from the core at intervals based on lithological variations and fracture distribution. All the samples were carefully chosen to avoid any fractures. The samples were oven dried at a temperature of 60°C for 72 hours to remove any moisture in the pore spaces. The dry weight and bulk volume of the plugs were measured, and the grain volume was measured based on gas displacement procedure of Bowel's Law (RP40). Helium porosimeter was used to measure the grain size of the samples and the matrix helium porosity of the selected samples was calculated from pore volume to the bulk volume ratio of each plug sample. The same group of plug samples that were used for measuring porosity were selected for measuring Klinkenberg-corrected matrix permeability (Klinkenberg, 1941; Rushing et al., 2004; Tanikawa and Shimamoto, 2006; Haines et al., 2016). Helium gas was used to measure steady state gas permeability (Ross, 2011). However, only the samples with porosity greater than 12% were measured using the steady state technique because below this value samples do not provide accurate results of the measured permeability (Rashid et al., 2015a and b; Rashid et al., 2017).

The fracture data was collected from cores and down hole image logs. A database of all measurable fracture parameters was collated recording fracture characteristics, dimensions, spacing, aperture, filling, frequency and orientation. (Gomez and Laubach, 2006; Guerriero et al., 2010; Rustichelli et al., 2016; Miranda et al., 2018). The fracture measurements are fully integrated with sedimentological data, conventional wireline logs and core analysis data to help define the fracture impact on the reservoir quality (Nelson, 1985; Laubach et al., 2009; Hou and Pan, 2013; Moumni et al., 2016; Bisdom et al., 2017).

Upon removal from the core barrels the core fractures were measured. The individual core pieces in each tray were correctly arranged and a reference line was drawn along the long axis of each core from top to the bottom which was used as a datum for the orientation measurement including apparent dip angle and direction of the fractures along the core samples. Upper Hemisphere stereonet pole plots and azimuth rose diagrams have been used for presenting the measured dip direction of sedimentary and tectonic features. Frequency dips angle histograms with various scales are used to characterize the dip and azimuth of sedimentary and tectonic features. Furthermore, fracture type, spacing, filling, length, aperture and termination were recorded for each fracture.

Image logs have been used for investigating fracture type, fracture orientation and parameters in reservoir rocks (Khoshbakht et al., 2012; Xu et al., 2016; Lai et al., 2017). The image logging tool used on this investigation was the X-tended Range Micro Image (XRMI) log tool which is a water-based mud micro-resistivity log which consist of 6 pads. The XRMI image log provides a vertical resolution of 0.1 inch (0.25 mm) and a depth of investigation of 0.95 inch (2.41 cm). The image logs were depth shifted relative to the GR log that was run with the XRMI tool simultaneously. Image interpretation of the both wells was processed using the Interactive Petrophysic (IP) software.

Image logs data were interpreted over the cored intervals in the well MW-2 and non-cored intervals in the wells MW-1 and MW-2. All visible fractures were recorded. The fracture orientations measured from the core intervals were compared with the image analysis using identifying fractures at different scales, and acceptable results were achieved from the core-log correlations (Russell et al., 2002; Folkestad et al., 2012; Brekke et al., 2017; Lai et al., 2018). Any difference between the measured parameters of fracture distribution gathered from the core and those of the borehole image data were subject to sensitivity analysis and the fracture measurements from the core intervals corrected accordingly (Goodall et al., 1998; Fontana et al., 2010; Nie et al., 2013).

Fracture types can be identified from image logs using resistivity contrast aspect between the rock matrix and the fracture filling. Open fractures, partially open mineralized fractures (partially cemented), cements veins and vuggy fractures are the dominant types of fractures that can be identified using well bore scan image data (Zazoun, 2013; Lai et al., 2013; Lai et al., 2017). In this study electrically conductive features represent fractures that cross-cut the rock matrix without displacement and were identified as open fractures. Low confidence electrically conductive features are comparable with open fractures (Serra, 1989; Ameen et al., 2012). The closed fractures and veins had high electrical resistance (light) images on the log (Ameen, 2016; Nian et al., 2017). Some fractures appeared poorly in the light band of the image log, these features were considered low confidence closed fractures. Furthermore, partially open mineralized fractures with vuggy porosity were identified on the image log as narrow alternating electrically resistive (bright) and electrically conductive (dark) bands (Table 2).

The fracture porosity and permeability in the cores was calculated based on the fracture length, aperture and frequency in the core interval (Howard and Nolen-Hoeksema, 1990). For the purpose of calculating the porosity value the core dimensions are considered to be one cubic meter of rock centered on the core, therefore the porosity is calculated every meter along the well bore. The porosity estimation is done by measuring the fracture aperture and fracture length in each meter of core. Each fracture family has a specific average aperture and frequency from which a void volume and "pore volume" can be calculated (eq. 1). The pore volume can then be used to calculate the fracture porosity in each one cubic metre of rock surrounding the borehole, over the entire borehole (eq. 2). This method takes into consideration fracture types, aperture and varying frequencies, as shown:

$$V_f = F_f \times F_a \times 1m^2 \qquad \text{(eq 1)}$$

$$\emptyset_f = \frac{V_{fn}}{1m^3} \qquad \text{(eq 2)}$$

V_f: *pore volume " void"*
F_f: *fracture frequency*
F_a: *fracture aperture*
V_{fn}: *space volume in n fracture family* $\emptyset_f$: *fracture porosity*

The aperture value of each fracture was considered as constant and the average distance was taken for each measurement. Only the effective opening was measured for calculating the fracture porosity. The accumulated porosity of all individual fractures and each fracture family were used to calculate fracture porosity. The Fracture permeability was calculated using the cubic law (Zimmerman et al., 1996). The fluid flow in the fracture is assumed laminar between two parallel plates separated by a constant distance "aperture" (Robin et al., 2018). The measured fracture permeability can be calculated using equation (3) (Jourde et al., 2002; Robin et al., 2018).

$$K_f = \frac{h^2}{12} \qquad \text{(eq 3)}$$

K_f: *fracture permeability*
h: *fracture aperture*

4 Results

4.1 Stratigraphy

This study focuses on the Aptian to Middle Turonian heterogeneous carbonate rocks of the Qamchuqa Formation in the Miran West field. This formation was first described at Qamchuqa Gorge in the Zagros Folded belt. The formation is about 800 m thick with an alternating dolostone and limestone lithology (van Bellen et al., 1959). It is stratigraphically split into Upper and Lower Qamchuqa Formations. The Upper Qamchuqa Formation consists of dolomitized argillaceous limestones and was deposited in a shallow marine environment during Albian Stage. The Lower Qamchuqa Formation consists of thickly bedded, argillaceous and fossiliferous limestones with silt size quartz and glauconite minerals. The limestone beds are intercalated with crystalline dolomite and occasionally laminated shale layers (Buday, 1980). The upper contact with the Kometan Formation is unconformable, while the lower contact with the Sarmord Formation is gradational at the type locality (van Bellen et al., 1959; Buday, 1980; Jassim and Goff, 2006; Aqrawi et al., 2010).

The total thickness of this formation is about 316 m in Well MW-1. The well MW-1 is dominated by deep marine facies of the Balambo Formation that extend as intercalations with the rock units of the Qamchuqa Formation. This phenomena is known to become more common toward the south-east fields of the Kirkuk embayment including the Jambur and Pulkhana fields, while toward south-west it becomes more recognizable as Qamchuqa rock units.

The total thickness of the Qamchuqa Formation is about 235 m in well MW-2, as it only consists of the rock units typical to the Qamchuqa Formation (Figure 3). Lithologically the formation is composed of interbedded limestones, dolostone and thin bedded claystones of various thicknesses.

The limestone beds of the Qamchuqa Formation in the Miran West field are light brown, occasionally dark brown becoming predominately grey brown in color in some intervals. The limestone rock units contain variable types of foraminifera and bioclasts. Furthermore, pyrite, glauconite and chert minerals are observed within the limestone beds. Thin argillaceous and organic rich laminations are frequently present from top to the bottom of the drilled intervals of the Qamchuqa Formation. These limestone are interbedded with mudstones and wackstones which have a hard and blocky structure with a micritic to microcrystalline matrices. They are light to medium grey and grey brown in colour, hard, blocky to sub-fissile, calcareous and pyritic. Occasionally packstones and dolostone occur randomly in the Qamchuqa intervals. The packstone dominate the limestone units they are light brown to beige to light pinkish brown in colour with a hard blocky structure that contains different types of fossils. The dolomite textures are fine crystalline, sucrosic matrixes with a grey to brown colour and hard microstructure.

4.2 Dynamic data

In the well MW-1 drilling was continuous in the Qamchuqa Formation without recording abnormal mud loss with a drilling mud weight of 10.5 ppg. Lost circulation was recorded at 1271 m, and total mud losses at 1283 m. The lost circulation was not recorded in the Qamchuqa Formation interval when using 10.5ppg of drilling mud. In the well MW-2 lost circulation was not recorded at the Qamchuqa Formation interval , while the losses were commenced in the Sarmord Formation at 1390m and increased rapidly down to 1430m MD (up to 100bbls/hr).

Drilling tests were carried out in the Qamchuqa Formation in both wells. DST#2 in well MW-1 provided inconsistent rates of gas. In well MW-2, DST#3 and #4 didn't record fluid flow, while DST#4 was recorded 5000 bwpd of the formation water flow in the Sarmord Formation interval.

4.3 Porosity and permeability

The porosity and permeability was measured from plug samples that were drilled from the non-fractured parts of the core in MW-2. The matrix porosities were measured using laboratory techniques of measured helium porosities which varied from 2.0% to 22.0%, with an average of 10% (Figures 4A, 5 and Table 3). The measured Klinkenberg-corrected matrix helium permeability was measured from plugs samples that have porosity measurements at ambient surface conditions in order to remove any effect of confining pressure on the permeability. The permeability ranged from 0.06 mD to 56.4 mD with the average value of 7.65 mD (Figure 4B and 5). The fracture porosities varied from 0.006% to 1.217% with the average of 0.173%. The fracture permeability varied from 1.22 mD to 1×10^{8} mD, with an average of 1.8×10^{6} mD. These results show the matrix porosity was higher than the fracture porosity but by contrast the fracture permeability was eight times higher than the matrix permeability.

4.4 Structure analysis

4.4.1 Core measurements

The structural analysis was carried out on the core from well MW-2, in the Qamchuqa Formation, this involved investigation of both sedimentary and tectonic features. The sedimentary features identified which are related to depositional environment and burial included bedding, burial stylolites and dissolution seams, while the tectonic features identified were tectonic stylolites, open fracture, partially open mineralized fractures, veins and faults.

Analysis of the bedding planes shows multi-directional azimuths; but this was because of the very low angle dips between 2° to 13° with an average of 5°. This suggests the bedding is horizontal or sub-horizontal with a possible slight trend a dipping to the east (Figure 7, A).

Some of the most common features identified in the core were the stylolites and dissolution seams. The stylolites and dissolution seams were observed throughout the majority of the formation especially in highly fractured zones. The amplitude of the stylolites varies from 2.0 mm to 40 mm. In total 478 stylolites have been recorded over the 112 m of core (Figure 6), 60% of them are burial stylolites. The burial stylolites are sub-horizontal with no dominant trending azimuth (Figure 7), although dips vary from the horizontal (0°) to sub-horizontal (13°) with an average dip of 6.8° confirming that they are most likely the result of burial stress with a principle vertical stress (σ^1). The stylolites were usually filled with residual clay, shale or calcite and occasionally bitumen was observed. The tectonic stylolites had dip directions which trended to the north-east, suggesting a principle horizontal stress (σ^1) of approximately NE-SW for them to develop. The dip varied from 20° to 90° with an average of 41.33° (Figure 7C).

Another sedimentary feature characterized were dissolution seams which were filled with residual clay and 348 of them were recorded over the length of the core. They were small scale features with a maximum length of 10.5 cm (Figure 7D). The dissolution seams are sub-horizontal and do not have any clear trending orientation, although the dip ranged from horizontal (0°) to sub-vertical (40°) the average dip was only 11°.

Over 350 partially open mineralized fractures and totally open fracture have been recorded from the Qamchuqa core. The fractures were mostly tensile in nature. The stratigraphic distribution of fractures was not even, with the majority recorded in the upper part of the core (Figure 8). On average the fracture density was about 3.5 fractures per meter which was slightly different when compared with result from image logs. The partially open mineralized fractures cross cut the burial stylolites and bedding planes or were slightly off-set by these sedimentary features suggesting they form contemporaneously or after the sedimentary features (Figure 9). These fractures were mostly partially filled by calcite or occasionally dolomite and organic matter (bitumen) (Figure 10).

The partially open mineralized fractures show a dominant ENE-WSW strike. The dips range from 6° to 90° with an average of 76° (Figure 11). Forming one sub-vertical fracture set dipping very steeply to the NNW. This is perpendicular to the Miran West fold axis and parallel to the main fault axis demonstrating the ENE-WSW compression. The fracture set represented by the partially open mineralized fractures can be interpreted as single family of steeply inclined fractures.

As shown in Figure 12 the effective opening (fracture aperture) of the partially open mineralized fractures was variable, fracture aperture varied from 0.1 mm to 10 mm with an average of 1.5 mm (Figure 13). The observed fractures length varied from 15 mm to 530 mm with an average length of 120 mm (Figure 14). Only a few fractures over 250 mm were visible. The wider fractures usually crossed the whole core and so fracture persistence measurements were limited to what was visible in the core. This means that many of the fractures have far greater persistence.

Over 250 veins were measured in the 112 m core (Figure 15). On average 2.5 vein features were identified every metre. The veins were usually fractures which are completely filled with calcite and closely associated and related to the partially open mineralized fracture in the upper part of the core. They either cross cut the bedding, burial stylolites and dissolution seams or terminate against them (Figure 15) and on occasion flow along the sedimentary features (Figure 15) demonstrating that the sedimentary structures formed before the veins and they are a contemporaneous or later tectonic feature. The thickness of the veins varied from 0.1 mm to 5 mm with an average of 0.7 mm (Figure 13). The lengths of the veins varied from 18 mm to 290 mm with an average of 95 mm but as with all linear features were frequently truncated by the core. The dip angle varies from 24° to 90° averaging 72°. The vein data shows similar trends to the partially open mineralized fractures with a dominant ENE-WSW strike, forming set one of very steeply dipping fractures to the NNW. The partially open mineralized fractures and the veins probably form from the same set of fractures or are part of the same tectonic event.

In the MW-2 well 25 drilling induced fractures were recorded occurring most commonly the highly fractured part of the core (Figure 16A). The dip angle varied from 28° to 88° with an average of 63°. The plotted fracture data illustrated a clear ENE-WSW (N75E) strike and these features were probably taking advantage of pre-existing weaknesses in the rock and potentially related to the main fracture orientation.

A fault zone was observed in the MW-2 core between 1130 m to 1147 m. The fault damage zone was characterized by slip surfaces of fault zones where cataclastic breakdown and hydrochemical modification of the rock has occurred. Adjacent to this on both sides a fracture damage zone was identified (Garland et al., 2010). Between 1130 - 1141 m the fault zone is associated with typical vuggy porosity due to dolomitisation with a possible hydrothermal origin (Figure 16B) (Kareem et al., 2016; Ghafur et al., 2019). The scale of this fault is 1 – 2 m thick at 1130 m to 1131 m (Figure 16B) and 1135m to 1137m (Figure 16C). The fault zone at 1130 - 1131 m and 1135 - 1147 m are probably part of the same basic fault zone associated with the interval of secondary dolomitisation approximately 25 m thick. Faults of 100 m displacement tend to have damage zones in the order of 10 m to 50 m wide, although there is wide scattering in the data because lithology and fault style. If the fault displacement is in the order of 10 m to 100 m. A 100 m displacement fault has a length reaching approximately 1000 m (Bech et al., 2001; Marrett and Allmendinger, 1990; Childs et al., 2009).

4.4.2 Image log analysis

The fracture sets were measured from the image logs, these covered a wider interval than the core. The MW2 core was 102 m in length whilst the image log is recovered all the drilled interval, 235 m in Well MW-2 and 355 m in well MW-1. The observed fracture density from the image logs were lower than the fracture distribution collected from the core. Over the intervals investigated from MW-1 and MW-2 wells, 81 electrical conductive features (open fractures), 61 partially open mineralized and 101 veins were recorded (Figure 17 and Figure 18). Furthermore, nine drilling conductive features that correspond to induced fractures and faults were observed from the image log analysis.

One of the challenges and complexities facing fracture analysis using the integration technique of image logs including FMI type and core data is difficulty in differentiation between open and partially open mineralized fractures in image logs. The second types occasionally appear as disconnected open fractures. Fracture thickness and the tool resolution quality are two factors which control the fracture observation certainty in the image logs. Furthermore, fracture filing and sedimentary features were also difficult to differentiate using FMI data. The fracture and fracture fill could be easily identified from core analysis.

The open fractures show two strikes the ENE-WSW strike orientations observed in the cores but also a set of fractures striking SE-NW which was not observed in the core (Figure 19). The measured dip angles are shallower compared to the core which potentially divides the fractures into conjugate set along each strike the reason for the different fracture styles moving from a sub-vertical fracture set in the cores to two sets of inclined conjugates fractures probably results from MW-1 (the borehole not cored) being on a different part of the anticlinal structure, closer to the fold axis and this is shown when the open fracture data to plotted separately for MW-1 and MW-2.

The partially open mineralized fractures and veins show trends which are very similar to the MW-2 borehole core striking of ENE-WSW; with both sets dipping steeply to the NNW (Figure 19).

The data plotted on stereonets and rose diagrams (Figures 19) show that the open and partially open mineralized fractures from the image logs are consistent in both wells MW-1 and MW-2. As stated in the previous paragraphs the main difference was in the fracture density and the quality of fracture observation that obtained from the log data analysis.

A number of veins were observed in the image logs. The strike orientation of the veins was ENE-WSW, very similar to the partially open mineralised fractures and the open fractures. The dip varied from 29° to 88° with an average of 67°.

Fracture spacing measured by the micro-resistivity image data was influenced by the image quality, especially over washed out intervals of the well, which resulted in poor fracture identification. The fracture intensities illustrated heterogeneous fracture distributions throughout the core. Open and partially mineralized fractures had an average apparent spacing of 0.26 m and veins had an apparent fracture spacing of 0.12 m over the continuous logging interval. The open fractures were commonly distributed in the upper part of the Qamchuqa Formation throughout both wells. This interval appeared as massive to laminated beds from the micro-resistivity image log.

The well intersected a fault-breccia at 1130 - 1137 m observed in cores of the Qamchuqa Formation. The orientation of the fault plane couldn't be determined with high confidence from the image log because of poor image quality. However, the position of a fault-breccia and damage zone could be seen on the image log in the well MW-1 (Figure 17 D) and the thickness of this zone was estimated at 24 m from the micro-resistivity image log. In well MW-1, total losses were encountered at 1285 m coinciding with a cluster of ENE-WSW striking fractures interpreted as a fault damage zone.

5 Discussion

5.1 Fracture paragenesis

Two main phases of fracture development have been identified as a result of the measurements from the core and micro-resistivity image logs. The first phase of development was syn-sedimentary that was penecontemporanous with early-late burial and diagenesis, followed by a second phase of fracture development associated with later tectonic activity and folding. The paragenetic pattern of the fractures growth was identified based on the fracture analysis and fracture relationships with the other sedimentary features (phase 1) and then fractures development by later tectonic activity (phase 2).

The burial stylolites and dissolution seams are sub-parallel to the bedding planes (horizontal to sub-horizontal) and formed as a result of depositional processes including pressure solution during burial with the features developing at depths shallower than 100 m (Tada and Siever, 1989; Gruzman, 1997) to deeper than 1 km (Scholle and Halley, 1985; Tada and Siever, 1989; Zhang and Spiers, 2005; Ebner et al., 2009; Agosta et al., 2009; Olierook et al., 2014; Lavenu et al., 2014; Yu et al., 2018). These features form when the maximum stress is vertical. These sedimentary features cause compression of the parent rock and development of different early fracture types. The sedimentary stylolites create local stress regimes that allow tension gashes and shear fractures to develop in the rocks (Aharonov and Karcz, 2019). Plannar, syn-burial extensional fractures initially formed perpendicular to the stylolites (Figure 20 A and B) and commonly terminate against the stylolite surfaces. The fracture surfaces are filled with dissolved carbonate matrix material formed from pressure solution. The fracture network and connectivity of this type of fracture is very poor and commonly sealed by the carbonate cement.

The early formed features considered to form as part of Phase 1 are the bedding, burial styolites and dissolution seams which are all sub-horizontal and related to lithostatic compression and compaction. Extensional fractures may also have started to form and infill. These types of fractures are possibly formed during Mesozoic specifically in the Aptian to Turonian. At this stage early ENE-WSW strike direction tensional fractures this stage early ENE-WSW strike direction tensional fracture may have formed, this corresponded with pressure solution and the fracture surfaces filled with the dissolved derived minerals.

The main stage of Phase 2 corresponds to a rotation of the horizontal compressive tectonic stress fields in the ENE-WSW direction, this fully develops the tensional fractures and the compressional regime fully develops the veins, partially open mineralized fractures, open fractures and tectonic stylolites who's orientation suggests a ENE-WSE compressional event. This stress enhanced the fracture apertures of open or partially-open fractures. The fractures strike to ENE-WSW forming during the Cretaceous to Miocene convergence of the Arabian and Iranian-

Eurasian plates. These types of fractures were parallel to the maximum horizontal stress (σ_H) during the convergences time and they are expected to be formed in the Late Cretaceous, Palaeogene and Miocene respectively. In addition these Phase 2 features cross cut the earlier sedimentary and burial features (Phase 1).

The late tectonic fractures including en-echelon planar to sigmoidal geometries tension shear gashes post-date the sedimentary stylolites and dissolution seams. The Phase 2 fractures have larger dimensions in comparison with the syn-sedimentary Phase 1 fractures. In addition, coarse spary calcite filled veins provide evidence of rapid fracture propagation for the post-burial tension gashes (Figure 20 C and D). The fracture geometries indicate rotational shear probably associated with fault deformation or local damage zones. Tectonic stylolites also formed in the core intervals by further pressure solution derived from the previously-created fractures (Yu et al., 2018; Mollema and Antonellini, 1996; Zubtsov et al., 2005; Croize et al., 2010; Fossen et al., 2011). The tectonic stylolites have steep angles of dip which are perpendicular to the dominant fracture orientations (Kim et al., 2004; Olierook et al., 2014). The tectonic stylolites run sub-parallel along the axis of the folds striking WNW-ESE which suggests they formed contemporaneously with folding in the region (Aschwanden et al., 2019). The faulting in the Cretaceous is linked to the compressive state of Zagros mountain construction (Garland et al., 2010) which was at its maximum in the Late Miocene to Pliocene time (Ameen, 1991). These fault probably formed due to outer arc extension in the Miran West field similar to the other structures in the Zagros folded belt (Awdal et al., 2013).

5.2 Fracture and reservoir quality

Fracture spacing and distribution have a significant role on in hydrocarbon migration and reservoir productivity in fractured carbonate rocks (Eichhubl and Behl., 1998; Aydin, 2000; Bourne et al., 2008). However, some types of fractures and burial features can have a negative impact on reservoir quality such as stylolites, dissolution seams and cemented fractures (Nelson, 1981; Burgess and Peter, 1985; Koepnick, 1987; Finkel and Wilkinson, 1990; Dutton and Willis, 1998; Olierook et al., 2014; Rashid et al., 2017). Burial stylolites, tectonic stylolites, veins and dissolution seams surfaces lined with residual clay, shale, calcite and occasionally bitumen all act as barriers for fluid flow and destroy the reservoir pore volume and connectivity. In the 112 m of core 750 stylolites and dissolution seams were recorded and 275 veins were recorded with the majority of the veins distributed around the stylolites and dissolution seams. This may suggest that the pressure solution calcite dissolved during the formation of the styolites and/or dissolution seams precipitated in open fractures creating the veins observed. The vein minerals usually consisted of calcite and occasionally dolomite minerals, these act to destroyed the reservoir quality. As a result, veins, stylolites and dissolution seams tend not to contain any hydrocarbons or allow hydrocarbon migration and act as fluid flow barriers for reservoir productivity. During the early stages of burial some types of these fractures may have had good reservoir quality but subsequent fracture formation, burial and tectonic processes have eventually destroyed reservoir potential specifically reducing the fracture interconnection and permeability of the rocks.

The magnitude of the porosity achieved from fractures can be considered as negligible except in some fracture zones with large scale fractures in terms of fracture aperture and fracture extension. The average fractured porosity was

0.173%, in some individual fractures these values are enhanced to 8% in highly fractured zones but these were not common over the studied interval. Furthermore, some macro size pores were observed in the core samples providing an increased reservoir porosity. However, the average measured matrix porosity is 10 times greater than what was recorded for the fracture porosity. Thus, fractures only have a minor impact on the reservoir porosity and the storage capacity of the reservoir rock, but in contrast, the fracture permeability has a significant positive impact on the reservoir quality.

The open and partially open mineralized fractures provided important fluid conduits between rocks of the reservoir with good matrix porosity. These Phase 2 fractures postdate and frequently crosscut the earlier Phase 1 syn-sedimentary stylolites and dissolution seams and interconnect the discontinuous fracture zones and subsequently enhancing the reservoir pore connectivity. From the core investigation two highly fractured permeable zones from 1085 m – 1095 m and 1105 m – 1130 m were observed in the core (Figure 8). In these zones the measured matrix and fracture permeabilities have 8 orders of magnitude difference; the average matrix permeability was 7.65 mD whilst the average fracture permeability was 1.8×10^{6} mD. Here, the magnitude of the fracture permeability is predominantly controlled by fracture spacing and fracture orientation. The interconnected fractures obviously enhanced the reservoir permeability.

The regional stress patterns in the Zagros folded belt is considered as the maximum horizontal stress has approximately the NE-SW directions (Reinecker et al., 2004; Vernant et al., 2004). The open fractures are preserved by the current in-situ stress regime which is sub-parallel with the dominant fractures direction. Conversely the fractures which run perpendicular to the current stress regime have closed apertures reducing the magnitude of the fracture permeability. The partially open mineralized fractures remain open whatever the current stress direction because the minerals bridge the apertures acting as structural beams preventing the aperture closing even when perpendicular to the maximum insitu stress orientation. However, the density of the sedimentary and tectonic features that reduced the reservoir quality are greater than the fractures which enhance reservoir quality. On average one meter of core contains 3.5 stylolites, 3.1 dissolution seams, 2.5 veins and 3.5 partially open mineralized fractures. But, the partially open mineralized fractures have an average thickness of 1.5 mm that is twice the thickness of the veins and much bigger than the stylolite and dissolutions seams thickness. Furthermore, average persistence of the partially open mineralized fractures is 120 mm in the core, whilst other features are less persistent for example veins are 90 mm. Consequently, the majority of the fractures are of a later tectonic origin (Phase 2) and cross-cut the early formed burial stylolites and dissolution seams (Phase 1). Thus, fracture aperture, fracture length and fracture timing of the partially open mineralized fractures controls the reservoir potential and improves matrix pore connectivity through fracture networks.

Faulting and fault deformations have a frequent impact on reservoir quality and specifically on fluid flow by creating an interconnecting network or by the development of mineralised zones which act as barriers to fluid migration (Curewitz and Karson, 1997; Aydin, 2000; Rotevatn et al., 2009).

There is a strong correlation between mud losses recorded while drilling and faulting in the Well MW-1 (Figure 21). The faulted rock and its associated damage zone observed in the Qamchuqa Formation at 1271 m – 1283 m coincides with mud losses and gas flow recorded during open hole testing (DST2). In contrast, in the Well MW-2 no mud losses were encountered at the around of the fault rock and its associated damage zone observed between 1129 m – 1154 m. This interval tested tight with open hole tests (DST3). These results imply that the fault zone does not have an effective permeability which may be due to limited reactivation or mineralization on the fault surface. However, core fault breccias were observed at 1130 m - 1140 m (Figure 17 B and C), while the fracture frequency and the fractured permeability are low in comparison with the other intervals over this well (Figure 8).

6 Conclusions

The outcomes of the investigation into the heterogeneous carbonate Qamchuqa Formation in Miran West block from the fracture analysis of core samples and micro-resistivity image log supplemented by the DST, RFT and Mud-Logging tool are as follows:

- The dominant sedimentary features observed from the studied intervals are represented by bedding, burial stylolites and dissolution seams. The tectonic features consist of open fractures, partially open mineralized fractures, veins, faults and tectonic stylolites. The sedimentary features are sub-horizontal with a very slight dip to the ENE, whilst the dominant tectonic fractures are very steeply inclined to vertical striking ENE-WSW, these are nearly perpendicular to the sedimentary features and to the principle horizontal stress to the NE-SW.
- The observed sedimentary and tectonic features are distributed heterogeneously from top to the bottom of the formations with at least two distinct episodes of fracture development and a complex structural history. The sedimentary stylolites and dissolution seams were formed at the early stages of burial diagenesis and consequently early fractures formed by stress derived

from stylolisation and dissolution seams (Phase 1), later tectonic activity produced several types of fractures that crosscut the earlier features (Phase 2).

- The stylolites, dissolution seams and veins have destroyed the matrix petrophysical properties including porosity and permeability of the reservoir formation. As the residual materials in the surfaces of stylolites and dissolution seams and the minerals that filled the fractures surfaces in the veins have occluded the pores and blocked the pore connectivity reducing the reservoir quality.

- The Phase 2 tectonic features including ENE-WSW dominant open fractures and partially open mineralized fractured orientation are perpendicular to the Miran West field axis and enhanced the reservoir permeability. The fracture permeability value is greater than the original matrix permeability by 8 orders of magnitude. Whilst, the fracture porosity has no impact on the reservoir quality as the original matrix porosity is 10 times greater than the fracture porosity.

- The fracture frequency, fracture aperture, fracture lengths and fracture timing are the main parameters that controlled the reservoir quality. Whilst some of the sedimentary and tectonic features act to reduce the reservoir quality the fracture aperture, length and origin enhanced reservoir quality controlling the reservoir potential and providing excellent fluid flow movement.

- The fault breccia associated with NE-SW striking hydrothermal vuggy fractures with no mud losses and no flow production was recorded while drilling suggesting that this structure is dynamically sealed in MW-2. In contrast, total mud losses and flow were recorded that coincided with a cluster of NE-SW striking vuggy fractures interpreted as damage zone of possibly faulting in MW-1.

Acknowledgements

The research data was provided by the Ministry of Natural Resources–Kurdistan Region Government, Iraq. We would like to thank the geology and administrations staffs from the ministry for selecting data set especially minerals and oil general directory.

References

Agosta, F., Alessandroni, M., Tondi, E., Aydin, A., 2009. Oblique normal faulting along the northern edge of the Majella Anticline, central Italy: inferences on hydrocarbon migration and accumulation. Journal of Structural Geology, 31, 674-690.

Agosta, F., Alessandroni, M., Antonellini, M., Tondi, E., Giorgioni, M., 2010. From fractures to flow: a field-based quantitative analysis of an outcropping carbonate reservoir. Tectonophysics,490, 197-213.

Aharonov, E. Karcz, Z., 2019. How stylolite tips crack rocks. Journal of Structural Geology, 118, 299–307.

Ahmadhadi, F., Daniel, J.-M., Azzizadeh, M., Lacombe, O., 2008. Evidence for prefolding vein development in the oligo-miocene asmari formation in the Centralzagros fold Belt, Iran. Tectonics 27, TC1016.

Alavi, M. ,2007. Structures of the Zagros Fold-Thrust Belt in Iran. American Journal of Science, 307, 1064-1095.

Al-Qayim, B. , Othman, D., 2012. Reservoir characterization of an intra-orogenic Carbonates platform: Pila Spi Formation, Taq Taq oil field, Kurdistan, Iraq. Geological Society, London, Special Publications, 370, 139-168.

Al-Qayim, B. , Rashid, F., 2012. Reservoir Characteristics of The Albian Upper Qamchuqa Formation Carbonates, Taq Taq Oilfield, Kurdistan, Iraq. Journal of Petroleum Geology, 35, 317-341.

Ameen, M. S. 1991. Alpine geowarpings in the Zagros-taurus range: influence on hydrocarbon generation, migration and accumulation. Journal of Petroleum Geology, 14, 417–428.

Ameen, M., MacPherson, K., Al-Marhoon, M., Rahim, Z., 2012. Diverse fracture properties and their impact on performance in conventional and tight-gas reservoirs, Saudi Arabia: The Unayzah, South Haradh case study. AAPG Bulletin, 96, 459-492.

Ameen, M. S., 2016. Fracture modes in the Silurian Qusaiba Shale Play, Northern Saudi Arabia and their geomechanical implications. Marine and Petroleum Geology,78, 312-355.

Aqrawi, A.A.M., Goff, J.C., Horbury, A.D., Sadooni, F.N., 2010. The Petroleum Geologyof Iraq. Scientific Press, Beaconsfield, p. 424.

Awdal, A.H., Braathen, A., Wennberg, O.P., Sherwani, G.H., 2013. The characteristics of fracture networks in the Shiranish formation of the Bina Bawi Anticline; comparison with the Taq Taq Field, Zagros, Kurdistan, NE Iraq. Petroleum Geoscince, 19, 139-155.

Aschwanden, L., Diamond, L.W., Adams, A., 2019. Effects of progressive burial on matrix porosity and permeability of dolostone in the foreland basin of the Alpine Orogen, Switzerland. Marine and Petroleum Geology, 100, 148–164.

Aydin, A., 2000. Fractures, faults, and hydrocarbon entrapment, migration and flow. Marine and Petroleum Geology, 17, 797-814.

Barker, S.L.L., Cox, S.F., Eggins, S.M., Gagan, M.K., 2006. Microchemical evidence for episodic growth of antitaxial veins during fracture-controlled fluid flow. Earth Planetary Science Letter , 250, 331-344.

Barr, D., Savory, K.E., Fowler, S.R., Arman, K., Mcgarrity, J.P., 2007. Pre-development fracture modelling in the Claire field, west of Shetland, Geological Society, London, Special Publications,270, 205-225.

Bech N., Bourgine, B., Castaing, C., Christensen,N.P., Frykamn, P., Genter, A., Gillespie, P.A., Hoier, C., Zinck-Jorgensen, K., Klinkby, L., Lanini,S., Lindgaard, H.F., Manzocchi, T., Middleton, M.F., Naismith, J., Odling, N.E., Rosendal, A., Siegal, P., Thrane, L., Trices, R., Walsh,J.J.,Wendling, J., 2001. Fracture interpretation and flow modelling in fractured reservoirs. Joule III, Europian commision , diroctorate-general XII,Science, research and development. No. JOF3-CT95-0015.

Becker, I., Koehrer, B., Waldvogel, M., Jelinek, W., Hilgers,C.,2018. Comparing fracture statistics from outcrop and reservoir data using conventional manual and t-LiDAR derived scanlines in Ca2 carbonates from the Southern Permian Basin, Germany, Marine and Petroleum Geology,95, 228-245.

Beydoun, Z.R., Hughes, C., Clark, M.W., Stonely, G., 1992. Petroleum in the Zagros Basin: a late Tertiary foreland basin overprinted onto the outer edge of a vast hydrocarbon rich Paleozoic-Mesozoic passive margin shelf. In: In: Macqueen, R., leckie, D. (Eds.), Foreland Basins and Fold-belts. American Association of Petroleum Geologists Memoir, 55, 309–339.

Bisdom, K., Bertotti, G., Bezerra, F.H., 2017. Inter-well scale natural fracture geometry and permeability variations in low-deformation carbonate rocks. Journal of structural geology , 97, 23–36.

Brekke, H., MacEachern, J.A., Roenitz, T., Dashtgard, S.E., 2017. The use of microresistivity image logs for facies interpretations: An example in point-bar deposits of the McMurray Formation, Alberta, Canada. AAPG Bulletin, 101(5), 655-682.

Bourne, S.J, Brauckmann, F. , Rijkels, L. , Stephenson, B.J. , Weber, A. , Willemse, E.J.M. , 2000, Predictive Modelling of Naturally Fractured Reservoirs using Geomechanics and Flow Simulation: Paper ADIPEC 0911 presented at the 9th Abu Dhabi International Petroleum Exhibition and Conference, Abu Dhabi, U.A.E., 10 p.

Buday, T., 1980. The Regional Geology of Iraq. In: Stratigraphy and Palaergeography,vol. 1. Publications of GEOSURV, Baghdad, p. 445.

Burgess, C.J., Peter C.K., 1985. Formation, distribution, and prediction of stylolites as permeability barriers in the Thamama Group, Abu Dhabi: Middle East Oil Technical Conference and Exhibition, 11–14 March , Bahrain.

Carminati, E., Aldega, L., Bigi, S., Corrado, S., D'Ambrogi, C., Mohammadi, P., Shaban,A., Sherkati, S., 2013. Control of Cambrian evaporites on fracturing in fault-related anticlines in the Zagros fold-and-thrust belt. International Journal of Earth Sciences, 102(5), 1237–1255.

Casini, G., Gillespie, P.A., Verg_es, J., Romaire, I., Fern_andez, N., Casciello, E., Saura, E., Mehl, C., Homke, S., Embry, J.-C., Aghajari, L., Hunt, D.W., 2011. Subseismic fractures in foreland fold and thrust belts: insight from the Lurestan Province, Zagros Mountains, Iran. Petroleum Geoscience, 17, 263-282.

Casini,G., Romaire, I., Casciello ,E., Saura,E., Vergés ,J., Fernández, N., Hunt,D.W.,2018. Fracture characterization in sigmoidal folds: Insights from the Siah Kuh anticline, Zagros, Iran. AAPG Bulletin, 102 (3), 369-399.

Childs, C. , Manzocchi, T., Walsh, J.J., Bonson,C.G., Nicol,A., Schöpfer, M. P.J., 2009. A geometric model of fault zone and faultrock thickness variations,Journal of Structural Geology,31(2),117-127.Conference and Exhibition, 11–14 March 1985, Bahrain.

Cooper, M., 2007. Structural style and hydrocarbon prospectivity in fold and thrust belts: a global review. Geological Society, Special publication , 272, 447-472.

Croize, D., Renard, F., Bjorlykke, K., Dysthe, D.K., 2010. Experimental calcite dissolution under stress: evolution of grain contact microstructure during pressure solution creep. Journal of Geophysical Research-Solid Earth 115.

Csontos, L., Sasv_ari, _A., Pocsai, T., K_osa, L., Salae, A.T., Ali, A., 2012. Structural evolution of the northwestern Zagros, Kurdistan Region, Iraq: implications on oil migration. GeoArabia ,17, 81-116.

Curewitz, D., Karson , J. A. ,1997. Structural settings of hydrothermal outflow: Fracture permeability maintained by fault propagation and interaction. Journal of Volcanology and Geothermal Research, 79, 149 – 168.

Dashti,R.,Rahimpour-Bonaba,H.,Zeinali,M., 2018. Fracture and mechanical stratigraphy in naturally fractured carbonate reservoirs-A case study from Zagros region . Marine and Petroleum Geology,97,466-479.

Dietrich, D., McKenzie, J.A., Song, H., 1983. Origin of calcite in syntectonic veins as determined from carbon-isotope ratios. Geology ,11, 547-551.

Dunham, R. J. ,1962. Classification of carbonate rocks according to depositional texture. In: Ham, W.E., ed., Classification of Carbonate rocks :AAPG-Publ-Memoris 1, Tulsa, Oklahoma., 108-121.

Ebner, M., Koehn, D., Toussaint, R., Renard, F., Schmittbuhl, J., 2009. Stress sensitivity of stylolite morphology. Earth and Planetary Science Letters,277, 394–398.

Eichhubl, P., Behl, R.J., 1998. Diagenesis, Deformation, and Fluid Flow in the Miocene Monterey Formation. The AAPG/SEPM Pacific Section Meeting in Venture, California. Special Publication 83.

Fakhari, M. ,Soleimany, B. , 2003. Early anticlines of the Zagros Fold Belt, South West Iran. Geological Society of America, Abstracts with Programs, 35, 341

Fard ,I.A., Braathen,A., Mokhtari, M., Alavi ,S.A.,2006. Interaction of the Zagros Fold–Thrust Belt and the Arabian-type, deep-seated folds in the Abadan Plain and the Dezful Embayment, SW Iran.Petroleum Geoscience, 12,347-362.

Folkestad, A., Veselovsky, Z., Roberts, P., 2012. Utilising borehole image logs to interpret delta to estuarine system: A case study of the subsurface Lower Jurassic Cook Formation in the Norwegian northern North Sea, Marine and Petroleum Geology, 29, 255-275.

Fontana, S, Nader , F.H., Morad ,S., Ceriani, A., Al-Aasm , I.S., 2010.Diagenesis of the Khuff Formation (Permian-Triassic), northern United Arab Emirates. Arabian Journal of Geoscience , 3, 351–68.

Fossen, H., Schultz, R.A., Torabi, A., 2011. Conditions and implications for compaction band formation in the Navajo Sandstone, Utah. Journal of Structure Geology, 33, 1477–1490.

Garland, C. R., Abalioglu, I., Akca, L., Cassidy, A., Chiffoleau, Y., Godail, L., Grace, M. A. S., Kader, H. J., Khalek, F., Legarre, H., Nazhat, H. B. , Sallier, B. ,2010. Appraisal and development of the Taq Taq field, Kurdistan region, Iraq. Geological Society, London, Petroleum Geology Conference series, 7, 801-810.

Garland, J., Neilson, J., Laubach, S. E., Whidden, K. J., 2012. Advances in carbonate exploration and reservoir analysis. Geological Society, London, Special Publications, 370, 1-15.

Ghafur, A.A., Hersi, O.S., Sissakian,V.K., Omer, H.O., Abdulhaq ,H.A.,2019. Facies-controlled dolomitization of the Lower Cretaceous Qamchuqa Formation, Kurdistan Region, Northern Iraq. Geoconvension , Calgary ,Canda , 13-17 May.

Gillespie, P., Monsen, E., Maerten, L., Hunt, D., Thurmond, J., Tuck, D., 2011. Fractures in carbonates: from digital outcrops to mechanical models. Outcrops revitalized—tools, techniques and applications: tulsa, Oklahoma. SEPM Concepts in Sedimentology and Paleontology ,10, 137–147.

Goodall, T. M. , Møller , N. K. , Rønningsl, T. M.,1998. The integration of electrical image logs with core data for improved sedimentological interpretation. Geological Society, London, Special Publications, 136, 237-248.

Gomez, L.A., Laubach, S.E., 2006. Rapid digital quantification of microfracture populations. Journal of structural geology , 28, 408–420.

Gruzman, Y. 1997. Origin of sedimentary stylolites from Israel. Unpublished M.Sc thesis, 877 Hebrew University.

Guerriero, V., Iannace, A., Mazzoli, S., Parente, M., Vitale, S., Giorgioni, M., 2010. Quantifying uncertainties in multi-scale studies of fractured reservoir analogues:

implemented statistical analysis of scan line data from carbonate rocks. J.ournal of structral geology , 32, 1271–1278

Haines , T.J., . Michie ,E. A.H , Neilson, J. E., Healy , D.,2016. Permeability evolution across carbonate hosted normal fault zones. Marine and Petroleum Geology, 72 , 62-82.

Haq, B.U., Hardenbol, J. , Vail, P.R., 1988. Mesozoic and Cenozoic chronostratigraphy and cycles of sea-level change. In: Wilgus, C.K., Hastings, B.S., Kendall, C.G.St.C., Posamentier, H., Van Wagoner, J. and Ross, C.A. (eds.), Sea-level changes: an integrated approach. SEPM, Special publication , 42, , 71-108.

Hertigae Company Ltd , 2009. Final Well Report , Well MW-1 , Miran licensed block , Kurdistan region , Iraq.

Hertigae Company Ltd , 2010. Final Well Report , Well MW-2 , Miran licensed block , Kurdistan region , Iraq.

Homke , S., Verges, J., Graces ,M., Emami ,H., Karpuz R.,2004. Magnetostratigraphy of Miocene–Pliocene Zagros foreland deposits in the front of the Push-e Kush Arc, (Lurestan Province, Iran). Earth Planetary Science Letter, 225 , 397-410.

Homke,S., Verge´s, J.,Serra-Kiel, J., Bernaola, G., Sharp, I., Garcés, M., Montero-Verdú, I., Karpuz, R., Goodarzi, M.H, 2009. Late Cretaceous–Paleocene formation of the proto-Zagros foreland basin, Lurestan Province, SW Iran. Geological Society of America Bulletin,121(7-8), 963-978.

Honarmand, J. , Amini, A., 2012.Diagenetic processes and reservoir properties in the ooid grainstones of the Asmari Formation, Cheshmeh Khush Oil Field, SW Iran, Journal of Petroleum Science and Engineering,81,70-79.

Howard, J..H , Nolen-Hoeksema, R.C. ,1990. Description of natural fracture systems for quantitative use in petroleum geology. AAPG Bulletin 74(2), 151–162.

Huntoon, P.W., Lundy, D.A., 1979. Fracture-controlled ground-water circulation and well siting in the vicinity of Laramie, Wyoming. Ground Water,17, 463-469.

Iranpanah, A. ,Esfandiari, B., 1979. Structural evolution and correlation of tectonic events in the Alborz Mountains, the Zagros Range and Central Iran. Bulletin de la Société belge de géologie, 88, 285-295.

Jassim, S.Z., Goff, J.C., 2006. The Geology of Iraq. Dolin, Prague, p. 341.

Joudaki, M. ,Farzipour-Saein, A. , Nilfouroushan , F., 2016. Kinematics and surface fracture pattern of the Anaran basement fault zone in NW of the Zagros fold–thrust belt.International journal of earth science, 105,869-883.

Jourde, H., Flodin, E.A., Aydin, A., Durlofsky, L.J. and Wen, X.H., 2002. Computing permeability of fault zones in eolian sandstone from outcrop measurements. AAPG bulletin, 86(7), 1187-1200.

Kareem, H.K., Al-Aasm,I.S., Mansurbeg, H.,2015. Structurally-controlled hydrothermal dolomitization: A case study of the Cretaceous Qamchuqa Formation, Zagros basin, Kurdistan Iraq. poster presentation at AAPG Education Directorate, Geoscience Technology Workshop, Carbonate Reservoirs of the Middle East, Abu Dhabi, UAE.

Khadivi, S., Mouthereau, F., Larrasoana , J.C., Verges , J., Lacombe, O., Khademi, E., Beamud, E., Melinte-Dobrinescu, M. , Suc, J.P. ,2010. Magnetochronology of synorogenic Miocene foreland sediments in the Fars arc of the Zagros Folded Belt (SW Iran). Basin Research , 22 (6), 918–932.

Khoshbakht, R., Salimi, A., Aski, H.S., Keshavarzi ,H. ,2012. Antibiotic Susceptibility of Bacterial Strains Isolated From Urinary Tract Infections in Karaj, Iran. Jundishapur journal of microbiology, 6(1), 86-90.

Kim, Y.S., Peacock, D.C.P., Sanderson, D.J., 2004. Fault damage zones. Journal of Structure Geology, 26, 503–517..

Klinkenberg, L. J. ,1941. The Permeability Of Porous Media To Liquids And Gases. American Petroleum Institute.

Koshnaw,R. I.,Horton, B. K., Stockli, D. F.,Barber, D. E.,Tamar-Agha, M. Y., Kendall, J. J. ,2017. Neogene shortening and exhumation of the Zagros fold-thrust belt and foreland basin in the Kurdistan region of northern Iraq. Tectonophysics, 694, 332–355.

Korneva, I. , Tondi, E. , Agosta, F. , Rustichelli, A. , Spina, V. , Bitonte, R. , Di Cuia, R,.2014. Structural properties of fractured and faulted Cretaceous platform carbonates, Murge Plateau (southern Italy),Marine and Petroleum Geology,57,312-326.

Lacombe, O., Bellahsen, N., Mouthereau, F., 2011. Fracture patterns in the Zagros Simply Folded Belt (Fars, Iran): constraints on early collisional tectonic history and role of basement faults. Geological Magazine,148, 940-963.

Lai, J., Wang, G., Zheng, X., Zhou, L., Xiao, C., Zhang, C., Wang, K. and Han, C., 2015. Recognition and evaluation method of fractures by micro-resistivity image logging in oil-based mud. Petroleum Geology and Recovery Efficiency, 22(6), 47-54.

Lai, J., Wang, G., Wang, S., Cao, J., Li, M., Pang, X., Han, C., Fan, X., Yang, L., He, Z., Qin, Z., 2018. A review on the applications of image logs in structural analysis and sedimentary characterization. Marine and petroleum geology, 95,139–166.

Lamarche, J., Lavenu, A.P.C., Gauthier, B.D.M., Guglielmi, Y., Jayet, O., 2012. Relationships between fracture patterns, geodynamics and mechanical stratigraphy in Carbonates (South-East Basin, France). Tectonophysics ,581, 231-245.

Lapponi, F., Casini, G., Sharp, I., Blendinger, W., Fernández, N., Romaire, I. , Hunt, D.W. 2011. From outcrop to 3D modelling: a case study of a dolomitized carbonate reservoir, Zagros Mountains, Iran. Petroleum Geoscience, 17, 283–308

Lavenu, A.P.C., Lamarche, J., Salardon, R., Gallois, A., Marie, L., Gauthier, B.D.M. ,2014.Relating background fractures to diagenesis and rock physical properties in a platform-slope transect. Example of the Maiella Mountain (central Italy). Journal of marine and petroleum geology, 51, 2-19.

Laubach, S.E., 2003. Practical approaches to identifying sealed and open fractures. AAPG Bulletin, 87, 561-579.

Laubach, S. E., Diaz-Tushman, K. , 2009. Laurentian paleostress trajectories and ephemeral fracture permeability, Cambrian Eriboll Formation sandstones west of the Moine thrust zone, northwest Scotland: Journal of the Geological Society (London), 166, 349–362.

Marrett, R., Allmendinger, R.W., 1990. Kinematic analysis of fault-slip data. Journal of Structural Geology, 12, 973–986.

Mcquillan, H. ,1973. Small-scale fracture density in Asmari Formation of SW Iran and its relation to bed thickness and structural setting. AAPG Bulletin, 57, 2367–2385.

Mcquillan, H. , 1974. Fracture patterns on Kuh-e Asmari Anticline, Southwest Iran. AAPG Bulletin, 58, 236–246

Miranda, T.S , Santos, R.F. , Barbosa, J.A. , Gomes, I.F. , Alencar, M.L., Correia, O.J.,Falcao, T.C. , Gale, J.F.W. , Neumann, V.H., 2018. Quantifying aperture, spacing and fracture intensity in a carbonate reservoir analogue: Crato Formation, NE Brazil. Marine and Petroleum Geology ,97 , 556–567.

Mollema, P.N., Antonellini, M.A., 1996. Compaction bands: a structural analog for antimode I cracks in aeolian sandstone. Tectonophysics, 267 (1), 209–228.

Motiei, H., 1993. Treatise on the geology of Iran: Stratigraphy of Zagros. Geological Survey of Iran, Tehran, pp 497.

Moumni, Y., Msaddek, M.Y., Chermiti,A., Chenini, I., Mercier, E., Dlala,M. 2016. Quantitative analysis of fractured carbonate reservoir and hydrodynamic implications: Case study of Horchane-Braga basin (central Tunisia). Journal of African Earth Sciences, 124, 311-322.

Narr, W., 1996. Estimating average fracture spacing in subsurface rock. AAPG Bulletun ,80 (10), 1565–1586.

Navabpour,P., Angelier,J., Barrier,E., 2007.Cenozoic post-collisional brittle tectonic history and stress reorientation in the High Zagros Belt (Iran,FarsProvince). Tectonophysics , 432,101–131.

Navabpour ,P. , Barrier,E.,2012. Stress states in the Zagros fold-and-thrust belt from passive margin to collisional tectonic setting. Tectonophysics , 581,76-83.

Nelson, R.A., 1981. Significance of fracture sets associated with stylolite zones. AAPG Bulleitin, 65, 2417–2425.

Nelson, R. A. 1985: Geologic analysis of naturally fractured reservoirs. Contribution Petroleum Geology and Engineering I, 279 pp.

Nelson, R.A., 2001. Geological Analysis of Naturally Fractured Reservoirs, second ed. Gulf Professional Publishing, Houston, 332pp.

Nemati, M., Pezeshk, H., 2005. Spatial distribution of fractures in the Asmari Formation of Iran in subsurface environment: effect of lithology and petrophysical properties. Natural Resource Research , 14, 305-316.

Neuzil, C.E., Tracy, J.V., 1981. Flow through fractures. Water Resources Research , 17 (1),191-199.

Nie, X., Zou, C., Pan, L., Huang, Z., Liu,D., 2013. Fracture analysis and determination of in-situ stress direction from resistivity and acoustic image logs and core data in the Wenchuan Earthquake Fault Scientific Drilling Borehole-2 (50–1370 m). Tectonophysics,593, 161-171.

Nian, T., Wang, G. , Song, H., 2017. Open tensile fractures at depth in anticlines: a case study in the Tarim basin, NW China. Terra Nova, 29(3), 183-190.

Olierook, H. K.H., Timms, N.E. ,P., Hamilton, J.,2014. Mechanisms for permeability modification in the damage zone of a normal fault, northern Perth Basin, Western Australia, Marine and Petroleum Geology,50,130-147.

Peacock, D.C.P., Harris, S.D., Mauldon, M., 2003. Use of curved scanlines and boreholes to predict fracture frequencies. , Structural Gology, 25, 109-119.

Peacock, D.C.P., Sanderson, D.J. and Rotevatn, A., 2018. Relationships between fractures, Structural Geology, 106, 41–53.

Pireh, A., Alavi, S.A., Ghassemi, M.R., Shaban, A., 2015. Analysis of natural fractures and effect of deformation intensity on fracture density in Garau formation for shale gas development within two anticlines of Zagros fold and thrust belt, Iran. Petroleum science and engineering, 125, 162–180

Rajabi ,M., Sherkati,S. , Bohloli ,B, Tingay,M.,2010. Subsurface fracture analysis and determination of in-situ stress direction using FMI logs: An example from the Santonian carbonates (Ilam Formation) in the Abadan Plain, Iran. Tectonophysics,492,192-200.

Rashid, F., Glover, P.W.J., Lorinczi, P., Collier, R. and Lawrence, J. 2015a. Porosity and permeability of tight carbonate reservoir rocks in the north of Iraq. Journal of Petroleum Science and Engineering, 133, 147-161.

Rashid, F., Glover, P.W.J., Lorinczi, P., Hussein, D., Collier, C and Lawrence J. 2015b. Permeability prediction in tight carbonate rocks using capillary pressure measurements, Marine and Petroleum Geology, 68, 536-550.

Rashid, F., Glover, P.W.J., Lorinczi, P., Hussein, D. and Lawrence, J., 2017. Microstructural controls on reservoir quality in tight oil carbonate reservoir rocks. Journal of Petroleum Science and Engineering, 156, 814-826.

Reif, D., Decker, K., Grasemann, B., Peresson,H.,2012. Fracture patterns in the Zagros fold-and-thrust belt, Kurdistan Region of Iraq. Tectonophysics, 576–577, 46-62.

Reinecker, J., Heidbach, O., Tingay, M., Connolly, P. and Müller, B., 2004. The 2004 release of the World Stress Map.

Ross, E. R., 2011. Grain's Petrophysical handbook: online shareware petrophysics Training and Reference manual.

Rotevatn, A., Fossen, H., Hesthammer, J., 2007. Are relay ramps conduits for fluid flow? Structural analysis of a relay ramp in Arches National Park, Utah Geoloical Asociation , special publication, 270, 55–71.

RP40, 1998. Recommended Practices for Core Analysis. 2nd ed. Washington, DC.

Russell, S. D., Akbar, M. , Badarinadh, V. , Walkden, G. M. , 2002.Rock types and permeability predictions from dipmeter and image logs: Shuaiba Reservoir, (Aptian), Abu Dhabi: AAPG Bulletin, 86, 1709-1732.

Rustichelli,A., Torrieri,S., Tondi, E., Laurita, S., Strauss, C., Agosta, F., Balsamo,F.,2016. Fracture characteristics in Cretaceous platform and overlying ramp carbonates: An outcrop study from Maiella Mountain (central Italy). Marine and Petroleum Geology,76,68-87.

Rushing, J. A., Newsham, K. E., Lasswell, P. M. & Balsingame, T. A., 2004. Klinkenberg-Corrected Permeability Measurements in Tight Gas Sands: Steady-State versus Unsteady-State Techniques. SPE 89867

Sattarzadeh, Y., Cosgrove, J.W. ,Vita-Finzi, C., 2000. The interplay of faulting and folding during the evolution of the Zagros deformation belt. In: Cosgrove, J.W. and Ameen, M.S. (eds.), Forced folds and fractures. Geological Societ of London, Special Publication, 169, 187-196.

Saura, E., Vergés,J., Homke,S., Blanc, E., Serra-Kiel,J.,Bernaola,G., Casciello,E Fernández, N., Romaire, I., Casini, G., Embry,J.C., ,I.R.,Hunt,D.W.,2011. Basin architecture and growth folding of the NW Zagros early foreland basin during the Late Cretaceous and early Tertiary. Journal of the Geological Society, 168, 235-250.

Scholle, P.A., Halley, R.B., 1985. Burial diagenesis: Out of sight, out of mind In: Schneidermann, N., Harris, P.M. (Eds.), Carbonate Cements, vol. 36. SEPM Special Publication, pp. 309–334.

Serra, O. ,1989. Formation MicroScanner image interpretation (p. 117). Schlumberger Educational Services.

Sherkati, S. Letouzey, J.,2004. Variation of Structural Style and Basin Evolution in the Central Zagros (Izeh Zone and Dezful Embayment) Iran. Marin and Petroleum Geology, 21, 535-554.

Singh, S.K., Akbar, M., Khan, B., Abu-Habbiel, H., Montaron, B., Sonneland, L., Godfrey, R., 2009. Characterizing fracture corridors for a large carbonate field of Kuwait by integrating Borehole data with the 3-D surface seismic. In: Adapted from Poster Presentation at AAPG Convention, Denver, Colorado, June 7-10.

Solano, N., Zambrano, L., Aguilera, R., 2011. Cumulative-gas-production distribution on the Nikanassin Formation, Alberta and British Columbia, Canada. SPE Reservoir Evaluation Engineerng , 14, 357-376.

Stephenson, B.J., Koopman, A., Hillgartner, H., Mcquillan, H., Bourne, S., Noad, J.J., Rawnsley, K., 2007. Structural and stratigraphic controls on foldrelated fracturing in the Zagros Mountains, Iran: implications for reservoir development. In: Lonergan, L.,Jolly, L. Lonergan, L., Jolly , R.J.H., Rawnsley, K., Sanderson, D.J., (eds),2007.

Fractured Reservoirs. Geological Society of London, Special Publication, number 270,285p.

Tada, R., Siever, R., 1989. Pressure Solution during Diagenesis. Annual Review of Earth and Planetary Sciences, 17, 89-118.

Talbot, C.J., Alavi, M., 1996. The past of a future syntaxis across the Zagros. Geological Society, London, Special Publications , 100, 89-109.

Tanikawa, W., Shimamoto, T., 2006. Klinkenberg effect for gas permeability and its comparison to water permeability for porous sedimentary rocks. Hydrology and Earth System Sciences. 3, 1315-1338.

Tavani, S., Storti, F., Soleimany, B., Fallah, M., Mu~noz, J.P., Gambini, R., 2011. Geometry, kinematics and fracture pattern of the Bangestan anticline, Zagros, SW Iran. Geological Magazine, 148, 964-979.

Tavani, S., Parente, M., Vitale, S., Iannace, A. , Corradetti, A., Bottini, C., Morsalnejad, D., Mazzoli, S., 2018. Early Jurassic rifting of the Arabian passive continental margin of the Neo Tethys. Field evidence from the Lurestan region of the Zagros fold - and- thrust belt, Iran. Tectonics,27, 2586-2607.

Thomas ,R.N., Paluszny ,A., Hambley ,D., Hawthorne ,F.M., Zimmerman,R.W.,2018. Permeability of observed three dimensional fracture networks in spent fuel pins . Journal of Nuclear Materials, 510 , 613-622.

van Bellen, R.C., Dunnington, H.V., Wetzel, R., Morton, D.M., 1959. Iraq. In: Dubertret, L. (Ed.), Lexique Stratigraphique International, 3, Asie. CNRS, Paris fasc 10a, 333.

Vernant, P.H., nilforoushan, F., hatzfield, D., abbassi, M.R., vigny, C., Masson, F., nankali, H., martinod, J., ashtiani, A., bayer, R., tavakoli, F., , Chery, J., 2004. Present-day crustal deformation and plate kinematics in the Middle East constrained by GPS measurements in Iran and northern Oman. Geophysical Journal International, 157, 381-398.

Versfelt Jr., P.L. 2001. Major Hydrocarbon Potential in Iran . AAPG Memoirs, 74, 417–427.

Wang, F., Li, Y., Tang, X., Chen, J., Gao, W., 2015. Petrophysical properties analysis of a carbonate reservoir with natural fractures and vugs using x-ray computed tomography.Jurnal of Natural Gas Science Engineering , 28, 215–225.

Wennberg, O.P., Svånå, T., Azizzadeh, M., Aqrawi, A.M.M., Brockbank, P., Lyslo, K.B., Ogilvie, S., 2006. Fracture intensity vs. mechanical stratigraphy in platform top carbonates: the Aquitanian of the Asmari Formation, Khaviz Anticline, Zagros, SW Iran. Petroleum Geoscience, 12, 235-245.

Wilson, C.E., Aydin, A., Karimi-Fard, M., Durlofsky, L.J., Sagy, A., Brodsky, E.E., Kreylos, O., Kellogg, L.H., 2011. From outcrop to flow simulation: constructing discrete fracture models from a LIDAR survey. AAPG Bulletin, 95, 1883–1905.

Xu , C.M., Cronin, T.P., McGinness , T.E., Steer, B.,2009. Middle Atokan sediment gravity flows in the Red Oak field, Arkoma Basin, Oklahoma: A sedimentary analysis using electrical borehole images and wireline logs, AAPG Bulletin, 93 (1), 1-29.

Yu, K., Cao,Y., Qiu,L., Sun,P., 2018.The hydrocarbon generation potential and migration in an alkaline evaporite basin: The Early Permian Fengcheng Formation in the Junggar Basin, northwestern China. Marine and Petroleum Geology, 98, 12–32.

Zazoun, R.S., 2013. Fracture density estimation from core and conventional well logs data using artificial neural networks: The Cambro-Ordovician reservoir of Mesdar oil field, Algeria. Journal of African Earth Sciences, 83, 55-73.

Zebari, M. ,2013 .Geometry and Evolution of Fold Structures within the High Folded Zone: Zagros Fold-Thrust Belt, Kurdistan region-Iraq, published MSc thesis , University of Nebraska.

Zebari, M. ,Burberry, C. M. 2015. 4-D evolution of anticlines and implications for hydrocarbon exploration within the Zagros Fold-Thrust Belt, Kurdistan Region, Iraq. GeoArabia, Gulf PetroLink, Bahrain,20, 161-188.

Zeeb, C., Gomez-Rivas, E., Bons, P.D., Blum, P., 2013. Evaluation of sampling methods for fracture network characterization using outcrops. AAPG Bulletin, 97, 1545–1566.

Zhang, X., Spiers, C.J., 2005. Compaction of granular calcite by pressure solution at room temperature and effects of pore fluid chemistry. International Journal of Rock Mechanics and Mining Sciences, 42(7-8), 950-960.

Zimmerman, R. W., Bodvarsson, G. S. ,1996. Hydraulic conductivity of rock fractures, Transport in porous media, 23, 1–30.

Zubtsov, S., Renard, F., Gratier, J.P., Dysthe, D.K., Traskine, V., 2005. Single-contact pressure solution creep on calcite monocrystals. Geology Society of London, Special Publication, 243 (1) 81–95.

List of Figures

Figure 1. Geologic map of the Kurdistan region and north of Iraq showing the study area and the locations of selected wells from Miran West block.

Figure 2. Stratigraphic summary of the Miran West structure, the lithologies were drawn based on core description, drilling cutting identification and wireline log analysis from the drilled wells (Heritage, 2009 and 2011).

Figure 3. Two sedimentary logs of the Qamchuqa Formation throughout the study area presented with the gamma ray deflection. The rock lithologies achieved from core, cutting and litho-log description of WM-1 and MW-2 wells.

Figure 4. Histograms of the magnitude of porosity measured throughout the studied core samples. The maximum measured matrix porosity was 22% (0.22) while the maximum fracture porosity was 1.2% (0.012) in the same formation.

Figure 5. Histograms of the measured permeabilities from the core samples including matrix and fracture permeabilities. The matrix porosity has a limited range from 0.010 mD to 20.26 mD. The fracture permeability is 5 orders higher than the maximum matrix permeability.

Figure 6. Stylolites and dissolution seam observed from the core samples of the Qamchuqa Formation in well MW-2. A: burial stylolites formed parallel to the bedding plane and have horizontal surfaces. B: tectonic stylolites have an inclined surface to the bedding plane with dip angle >40°. C: dissolution seams formed parallel to the bedding plane and sedimentary stylolites.

Figure 7. Stereonets pole plots, rose diagrams and frequency dip angle histograms of bedding plane, stylolites and dissolution seams achieved from core samples in well MW-2. A_1: Stereonet azimuth of bedding planes. A_2: rose diagram of bedding planes . A_3: frequency dip angle of bedding planes. B_1: Stereonet azimuth of burial stylolites. B_2: rose diagram of burial stylolites .B_3: frequency dip angle of burial stylolites. C_1: Stereonet azimuth of tectonic stylolites. C_2: strike rose diagram of tectonic stylolites. C_3: frequency dip angle of tectonic stylolites. D_1: Stereonet azimuth of dissolution seam. D_2: Azimuth rose diagram of dissolution seam. D_3: frequency dip angle of dissolution seam.

Figure 8. A: Fracture density (number of fractures) achieved from the core samples as a function of the core depth in well MW-2. The fracture concentrations in the

upper part of the core samples are much higher from the lower part. **B**: Magnitude of measured fracture permeability frequency as a function of the core depth.

Figure 9. Termination of partially open mineralized fractures by different sedimentary features. A: parallel en echelon partially open mineralized fractures terminated by bedding plane .B: en echelon partially open mineralized fractures terminating against stylolites. C: partially open mineralized fracture cross cutting the whole sample.

Figure 10. Types of in-filling of partially open mineralized fractures. A: partially open mineralized fracture surface filled with calcite mineral. B: partially open mineralized fracture surface filled with calcite and dolomite minerals mineral. C: partial open minerlized fracture surface filled with calcite and dolomite minerals with residual bitumen.

Figure 11. Stereonets, pole plot, rose diagrams and frequency dip angle histograms of fractures measured from core samples in MW-2 . A_1: stereonet of partially open mineralized fractures .A_2: azimuth rose diagram of partially open mineralized fractures .A_3: frequency dip angle of partially open mineralized fractures. B_1: stereonet of induced fractures. B_2: azimuth rose diagram of induced fractures. B_3: frequency dip angle of induced fractures. C_1: streonet of veins .C_2: azimuth rose diagram of veins .C_3: frequency dip angle of veins.

Figure 12. Fracture opening (aperture) scale of partially open mineralized fractures selected from available core samples of Qamchuqa Formation in well MW-2. The fracture apertures have variable scales.

Figure 13. Histogram of fracture aperture of partially open mineralized fractures and veins of the Qamchuqa Formation.

Figure 14. Histogram of fracture lengths of partially open mineralized fractures and veins of the Qamchuqa Formation.

Figure 15. Veins in the cored interval collected from the Qamchuqa Formation in MW-2 well. A: post-dated stylolites and veins, B: post-dated dissolution seams and the veins terminating at a dissolution seam at the upper part of the core sample, C: vein formed before stylolisation.

Figure 16. Different fractures related rocks observed within the core samples. A: induced fracture formed by drilling. B: Crushed-fault breccias recorded in the lower part of the Qamchuqa Formation in MW-2 well, interval 1130 – 1140 m. C: macro vug hydrothermal fault related pores recorded in the fracture zones, interval 1130 – 1140 m.

Figure 17. Micro-resistivity image log (XRMI) images of MW-2 well selected from different interval to show various types of fractures. A: electrically conductive and resistive features of en echelon partially open mineralized fractures. B: continuous conductive electric path of opened fractures. C: high resistivity of veins. D: patches of conductive and resistive electrical images show fault breccias.

Figure 18. Micro-resistivity image log (XRMI) images of MW-1. The images cropped from different interval to show various types of fractures. A: electrically high conductive images of open fractures. B: conductive and resistive features of partially open mineralized fractures. C: mixtures of conductive and resistive electrical images show faulted rocks, total loss of the drilling mud was recorded in this interval. D: High angle and nearly vertical conductive features of induced fractures.

Figure 19. Stereonets pole plots, rose diagrams and frequency dip angle histograms of fractures measured from XRFI images. A_1: streonet of electrically conductive (open) fractures. A_2: azimuth rose diagram of electrically conductive (open) fractures .A_3: frequency dip angle of electrically conductive (open) fractures. B_1: azimuth stereonet of partially open mineralised fractures. B_2: azimuth rose diagram of partially mineralised fractures. B_3: frequency dip angle of partially open mineralised fractures. C_1: stereonet of electrically conductive induced fractures. C_2: azimuth rose diagram of electrically conductive induced fractures. C_3: frequency dip angle of electrically conductive induced fractures. D_1: stereonet of electrically resistive veins .D_2: azimuth rose diagram of electrically resistive veins .D_3: frequency dip angle of mineralised fractures.

Figure 20. Stylolite, dissolution seam and vein relationships. A: fractured formed perpendicular to the dissolution seam during burial stage. B: partially open mineralized fracture perpendicular to the surface of the stylolites. C: fractures post-date to the stylolite surfaces and the fracture surface filled with coarse calcite crystals. D: Veins and partially open mineralized crossing stylolite and dissolution seam surfaces, formed by tectonic activity.

Figure 21. Mud losses as a function of the drilled depth of MW-1 and MW-2. The figure contains test results and the position of fault zone in the studied wells.

List of Tables

Table 1 Summary of the collected data from the Miran West field.

Table 2 Definition and features used for fracture identification from micro-resistivity image logs.

Table 3 Porosity and permeability results.

Figure 1

Click here to download high resolution image

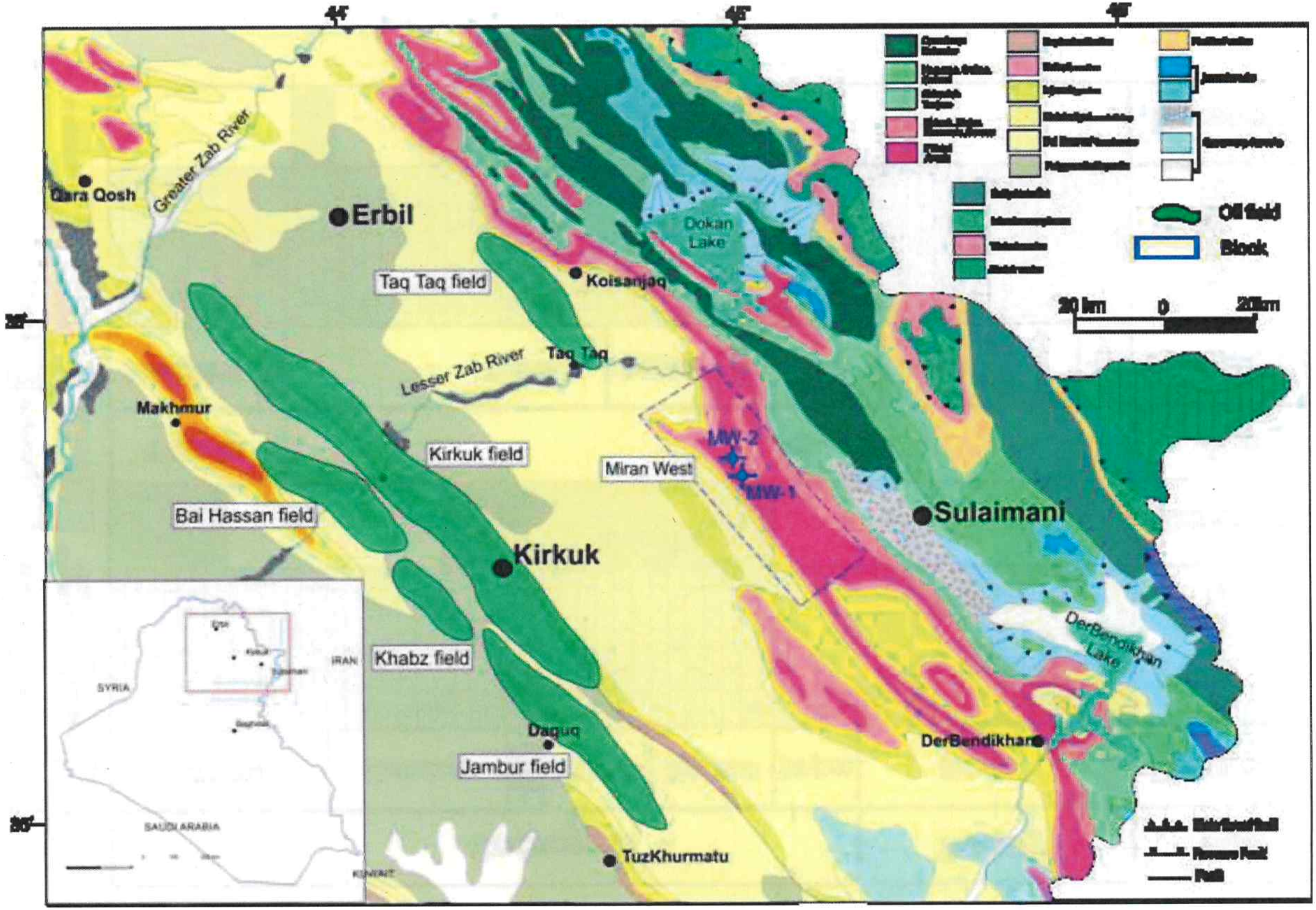

Figure 2

Click here to download high resolution image

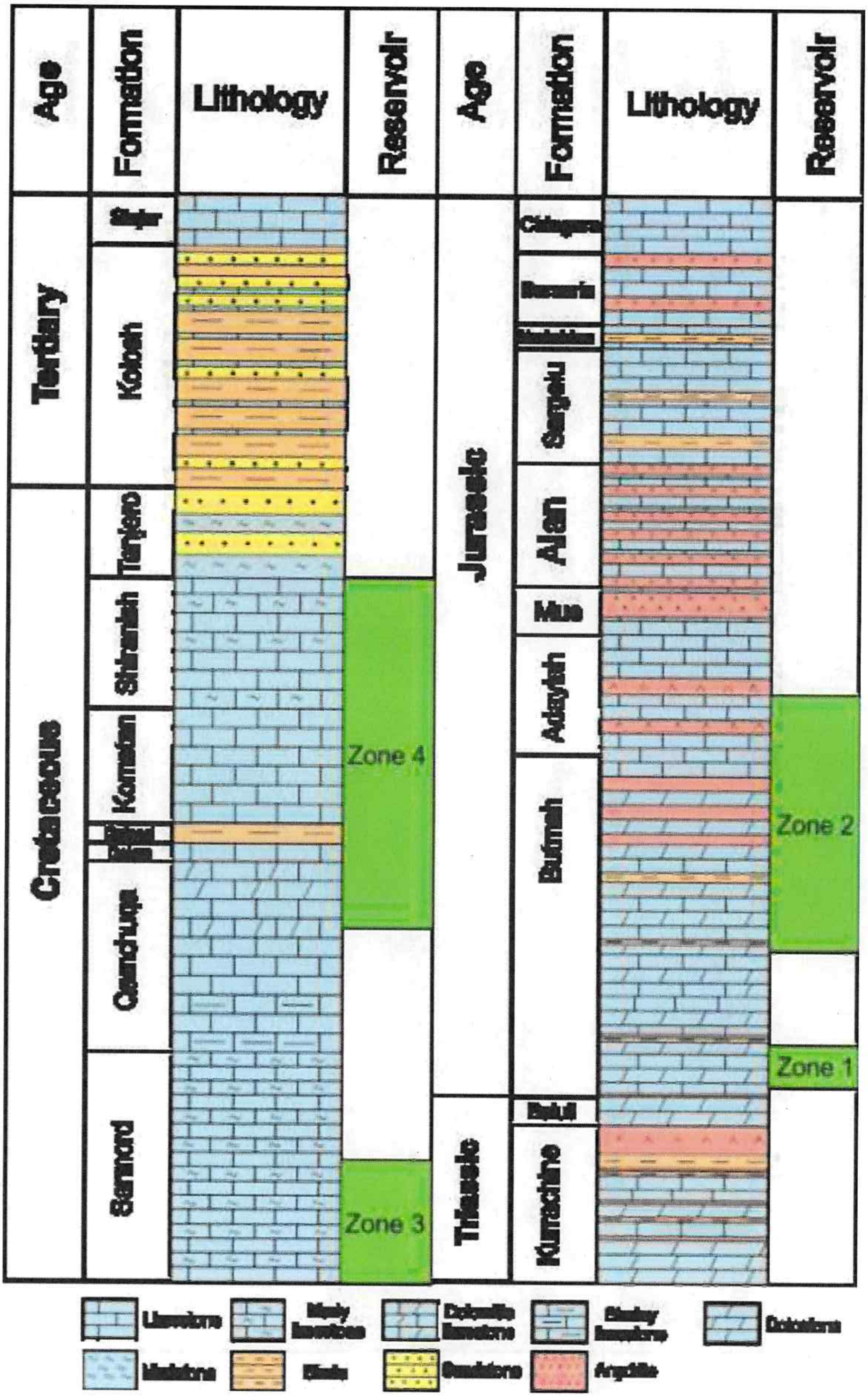

Figure 3

Click here to download high resolution image

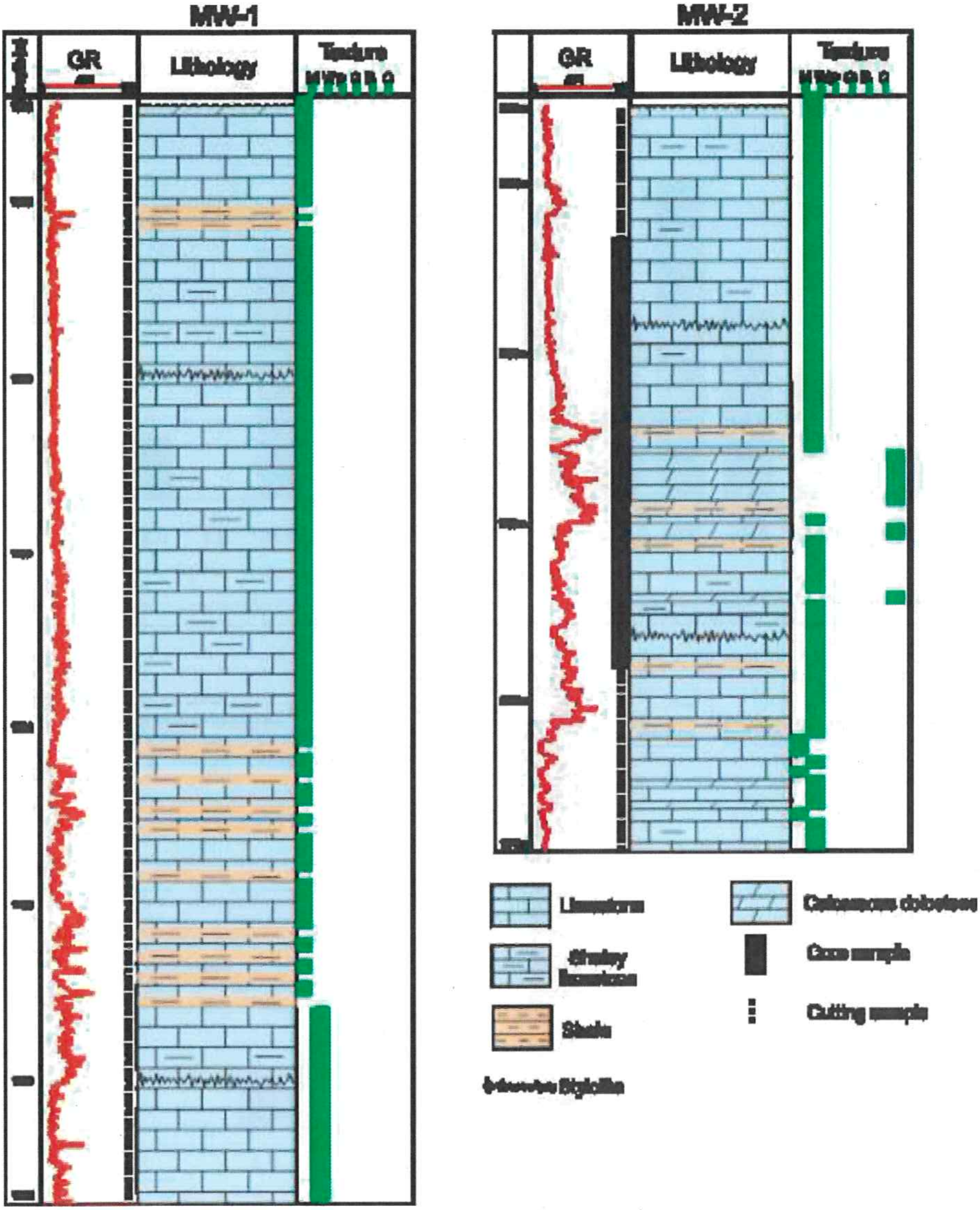

Figure 4
Click here to download high resolution image

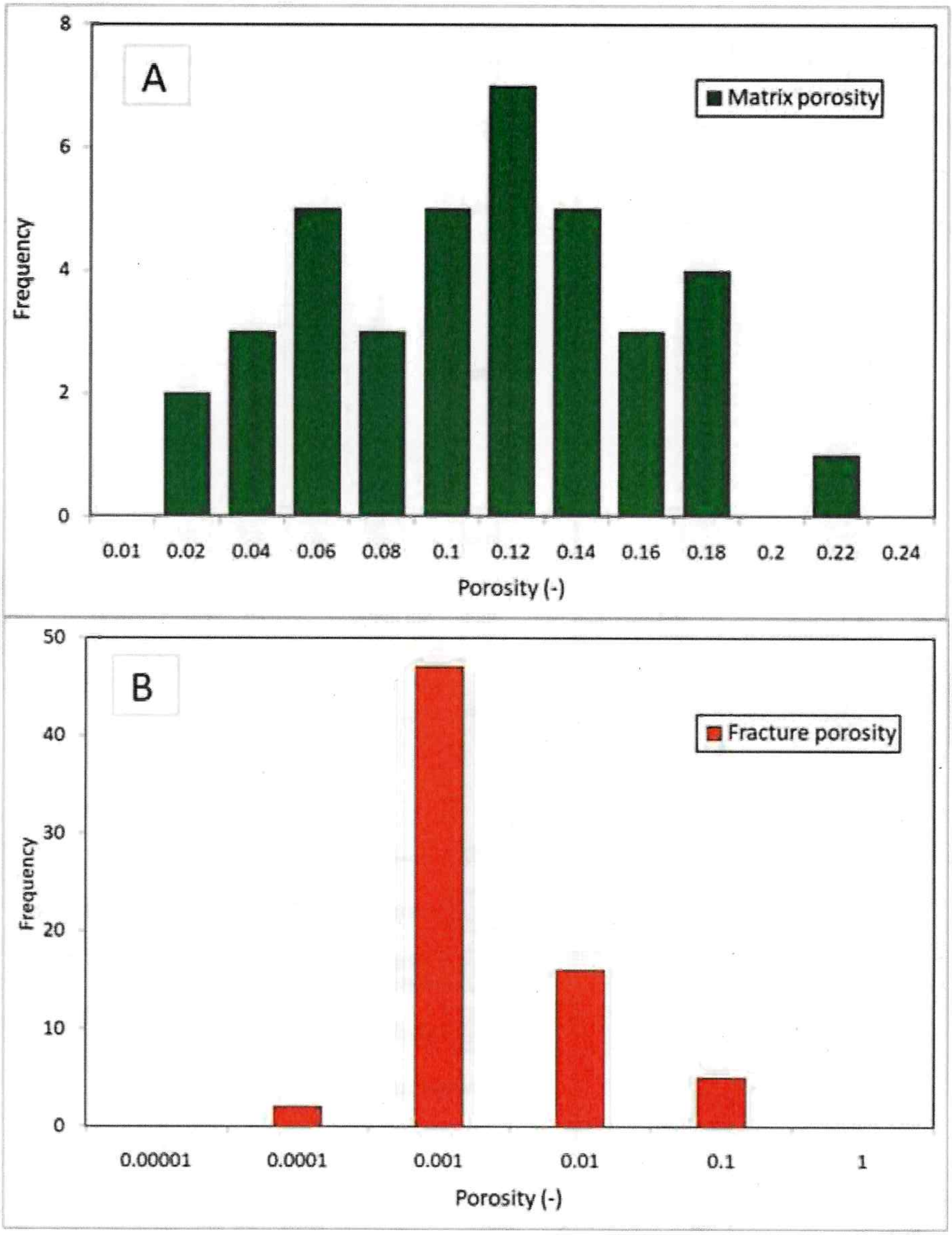

Figure 5

Click here to download high resolution image

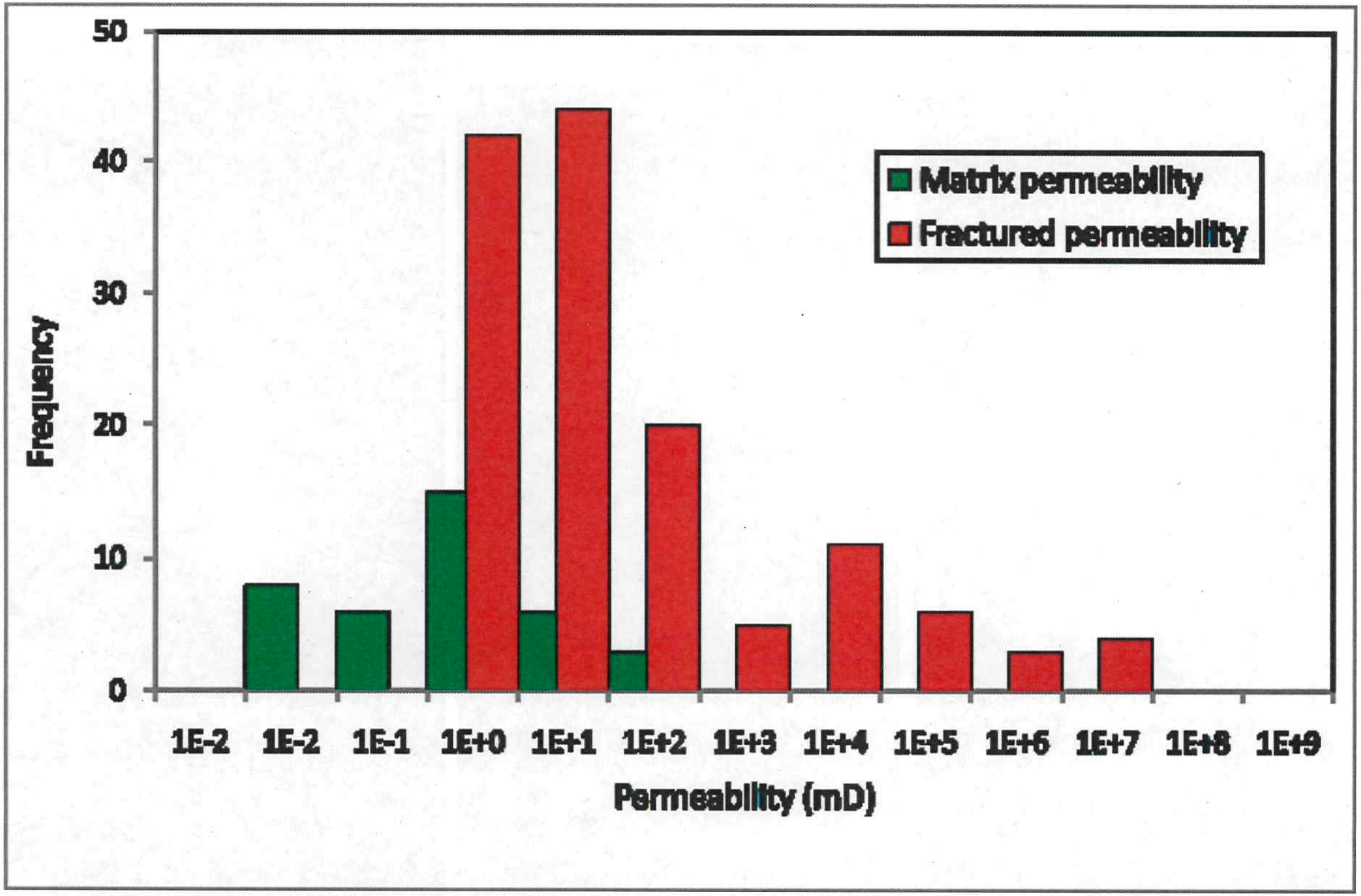

Figure 6
Click here to download high resolution image

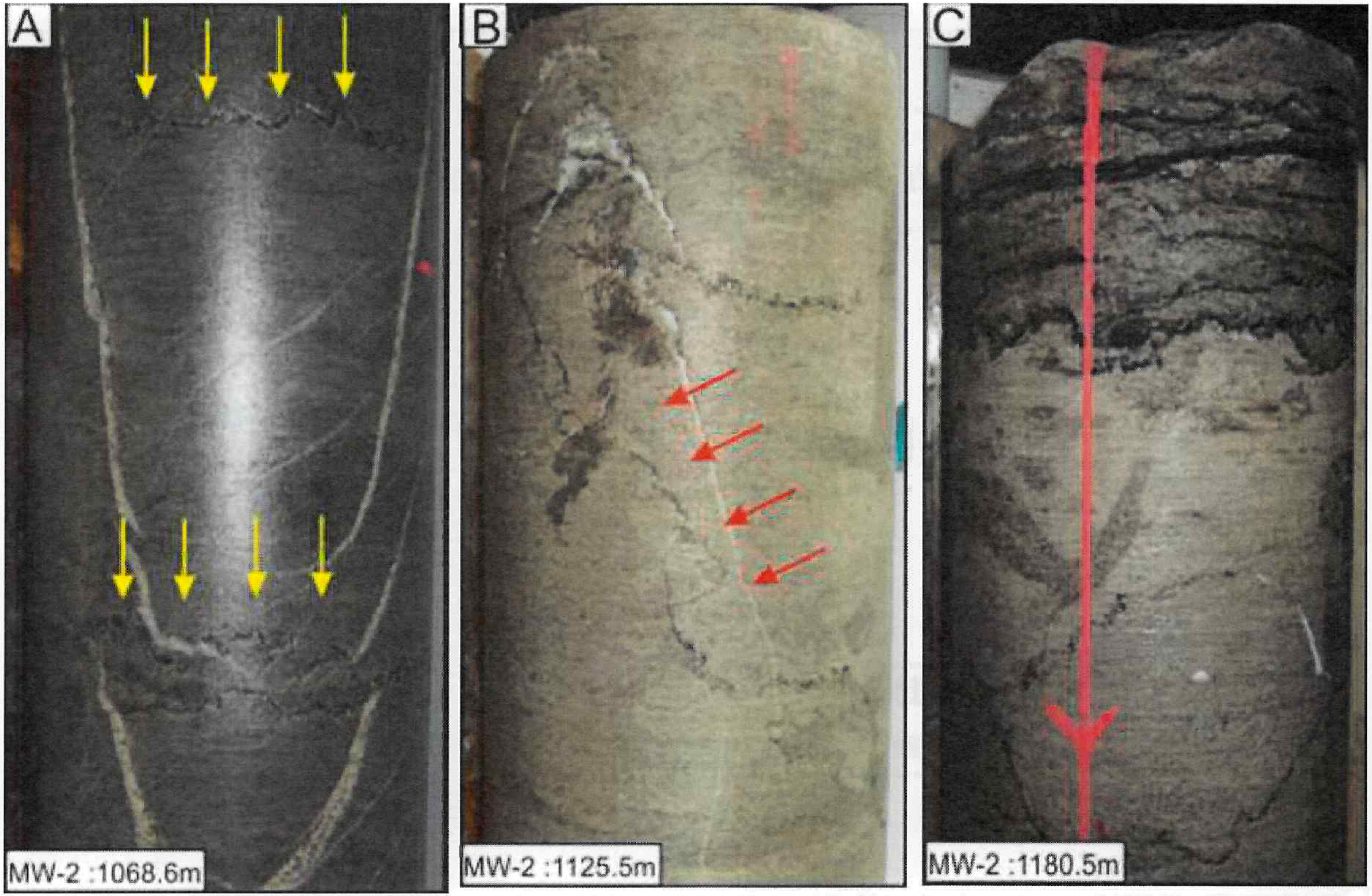

Figure 7
Click here to download high resolution image

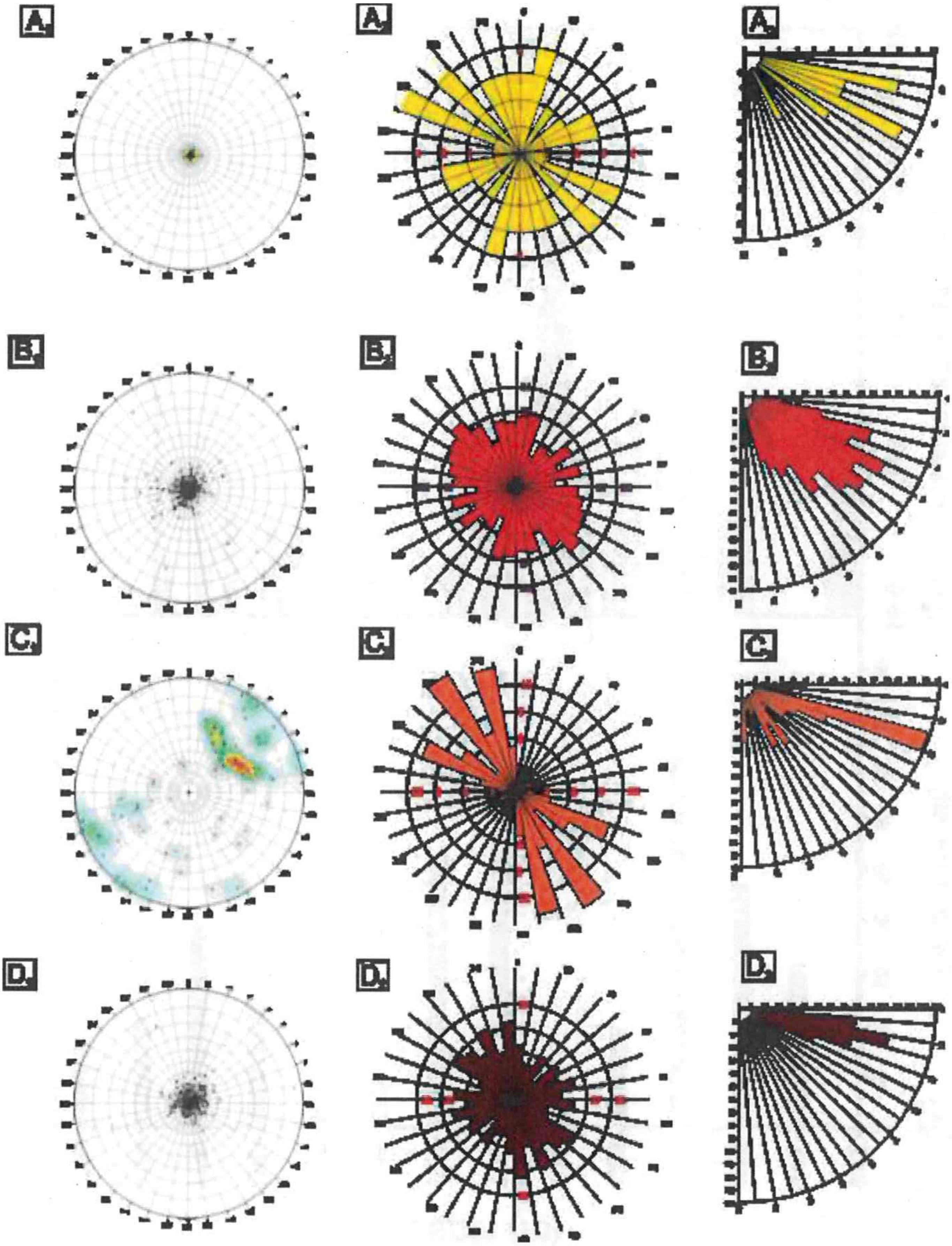

Figure 8

Click here to download high resolution image

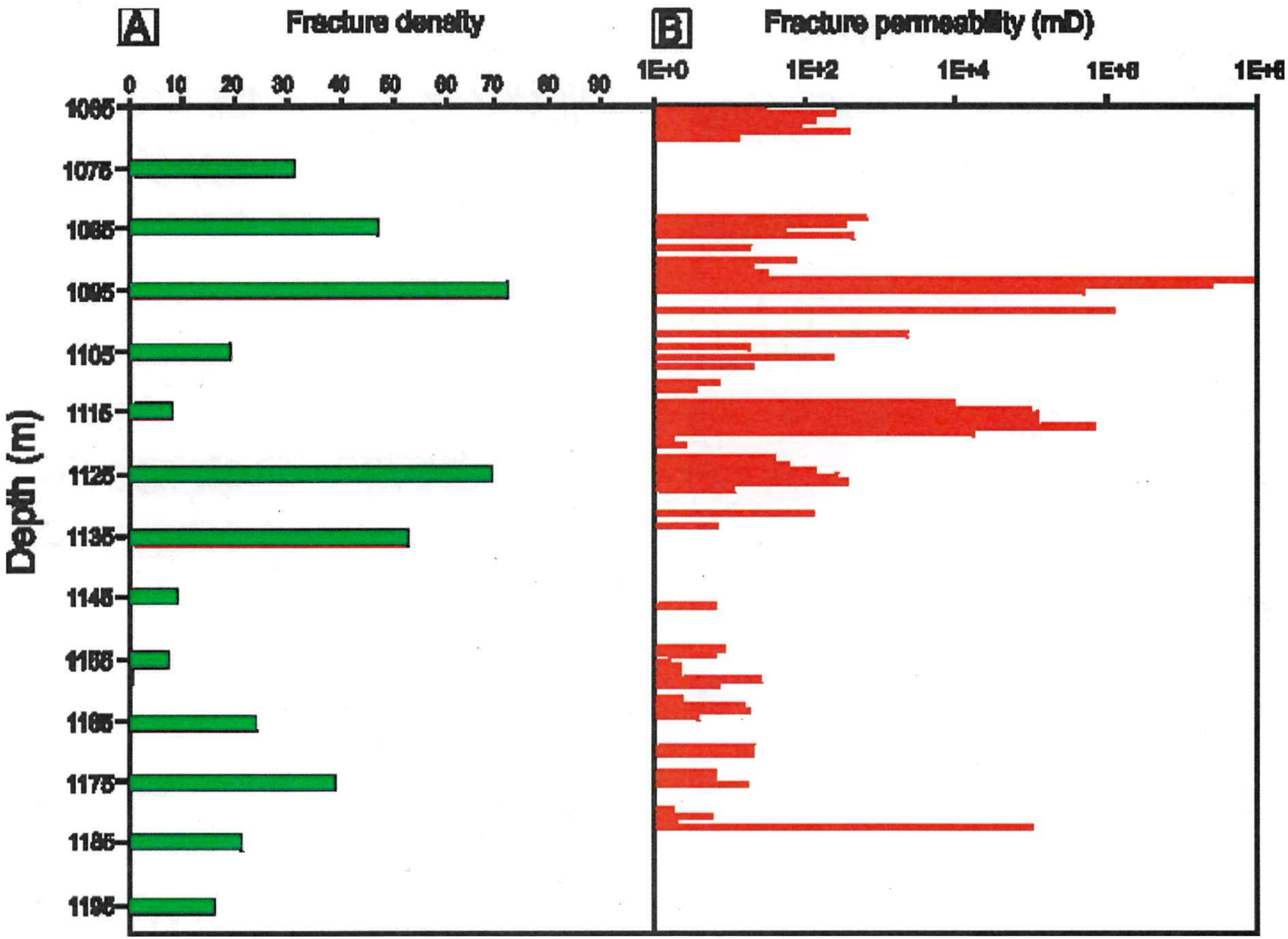

Figure 9
Click here to download high resolution image

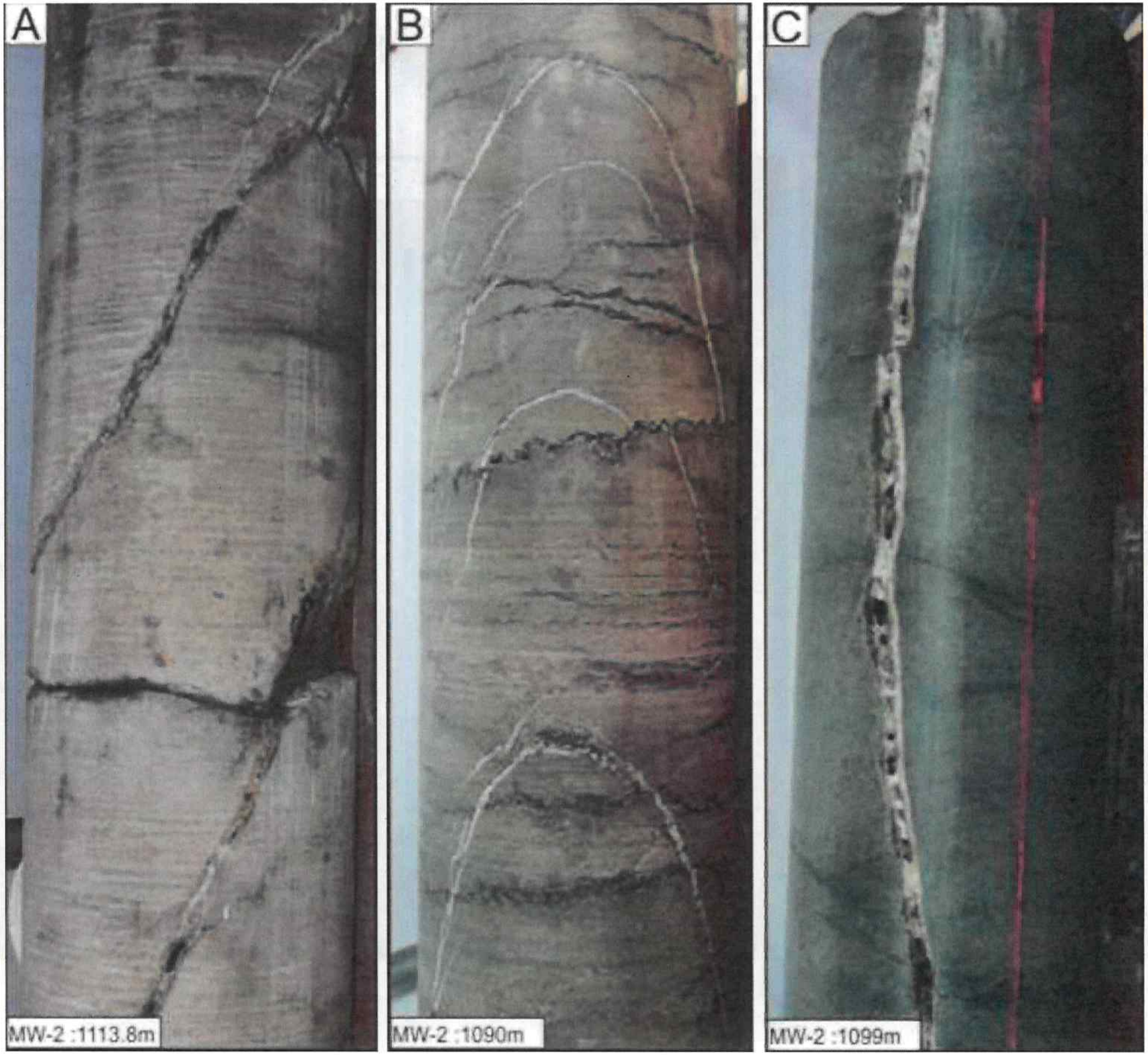

Figure 10
Click here to download high resolution image

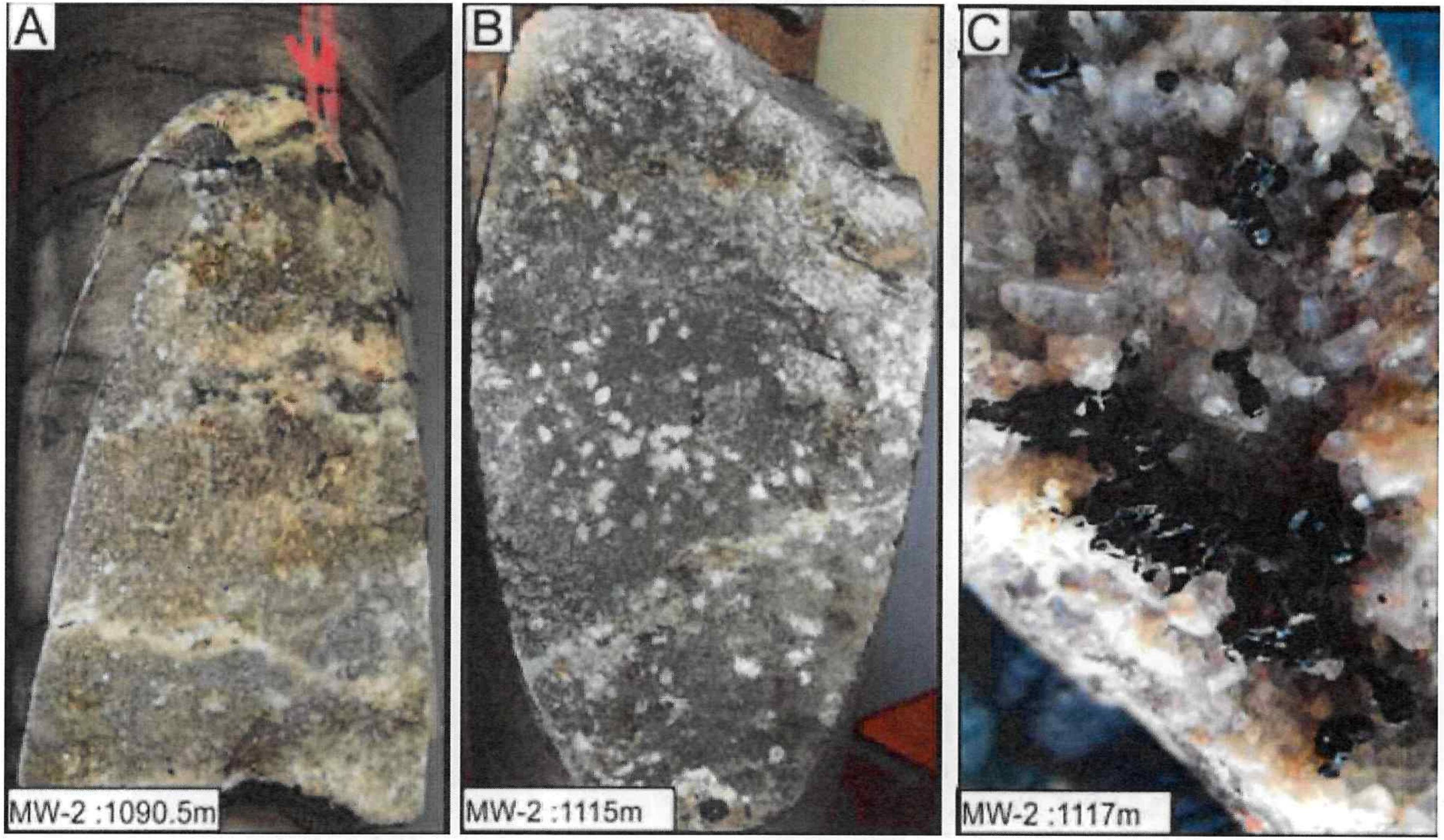

Figure 11

Click here to download high resolution image

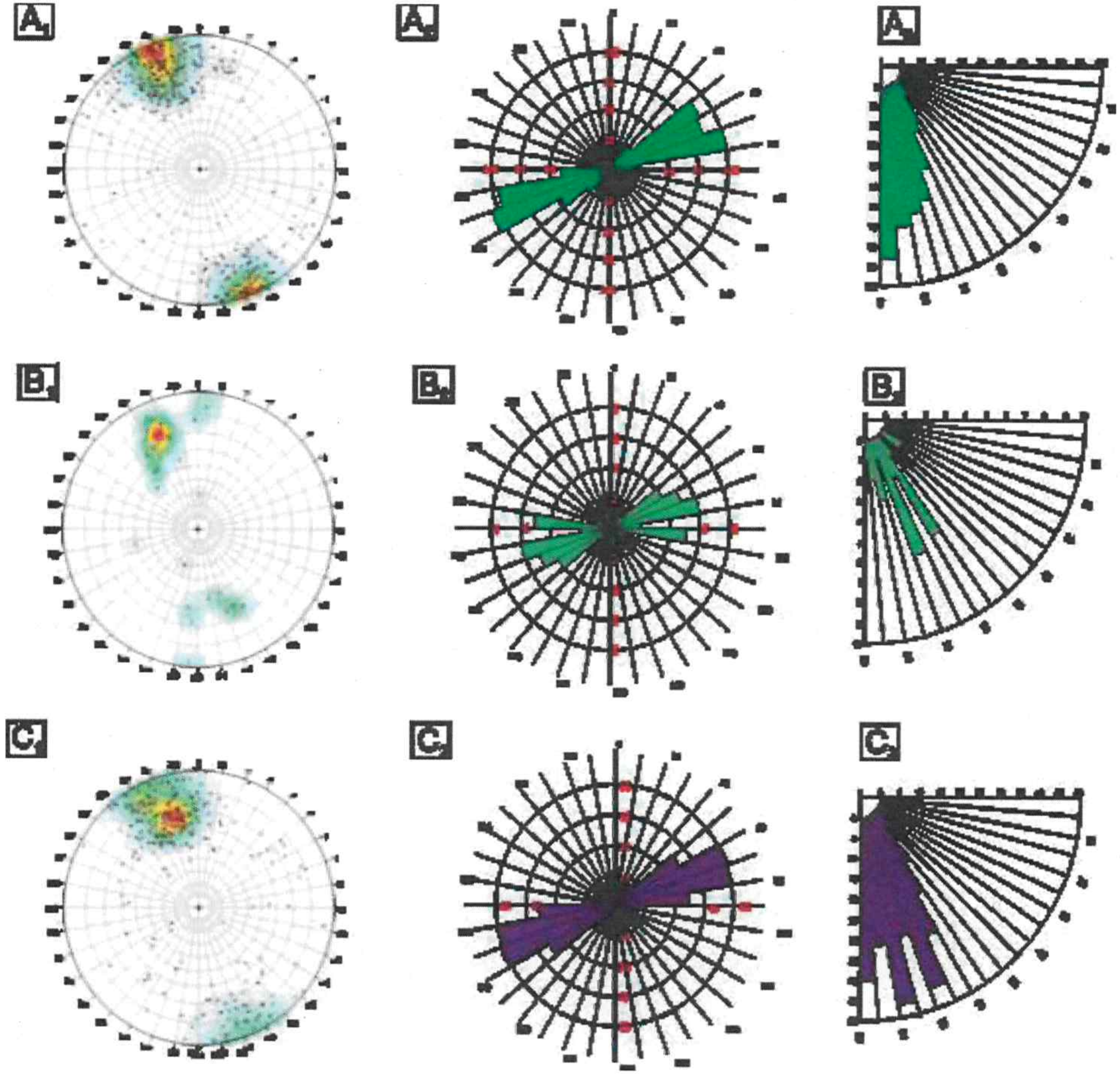

Figure 12
Click here to download high resolution image

Figure 13

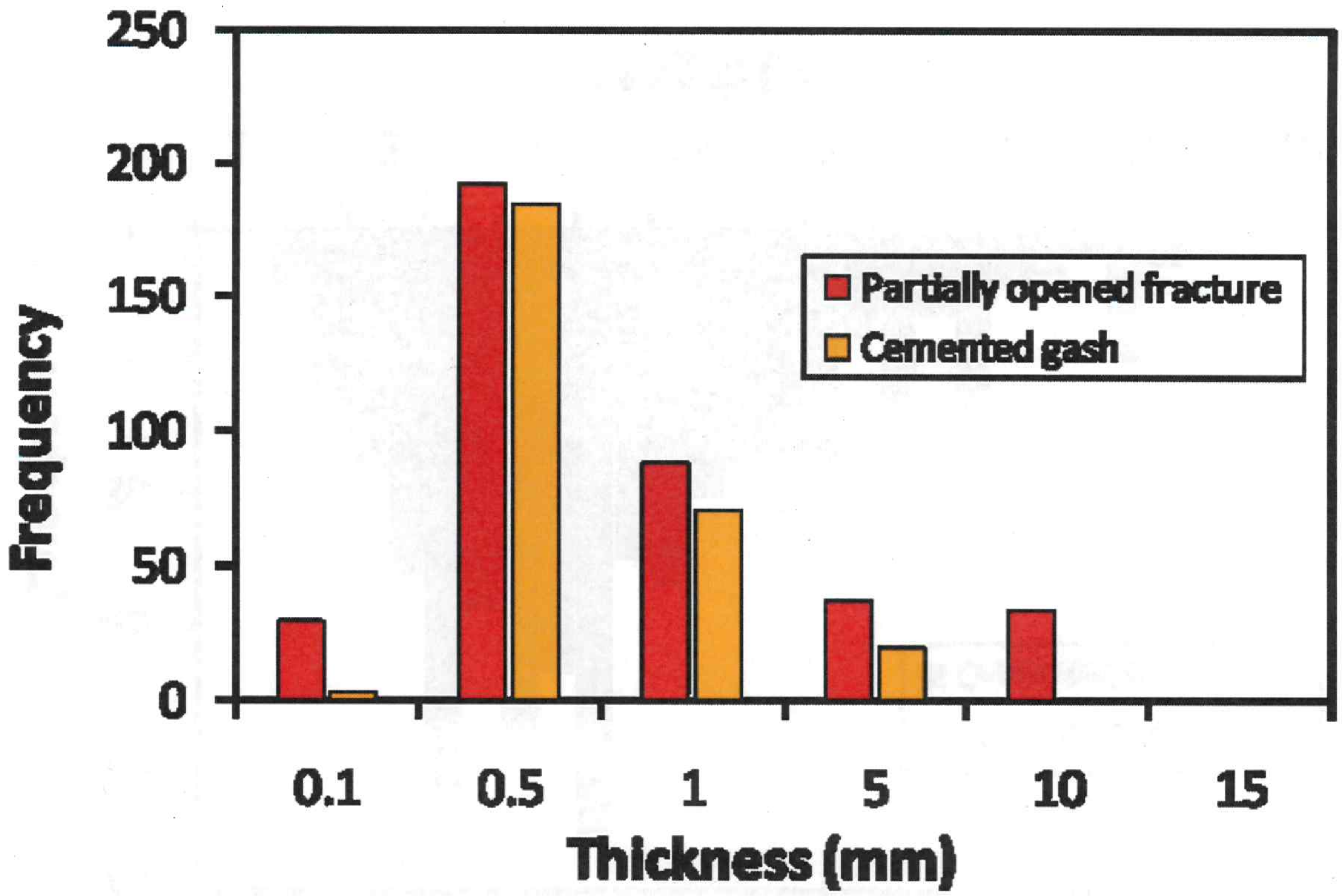
Frequency
250
200
150
100
50
0
0.1
0.5
1
5
10
15
Thickness (mm)
Partially opened fracture
Cemented gash

Figure 14

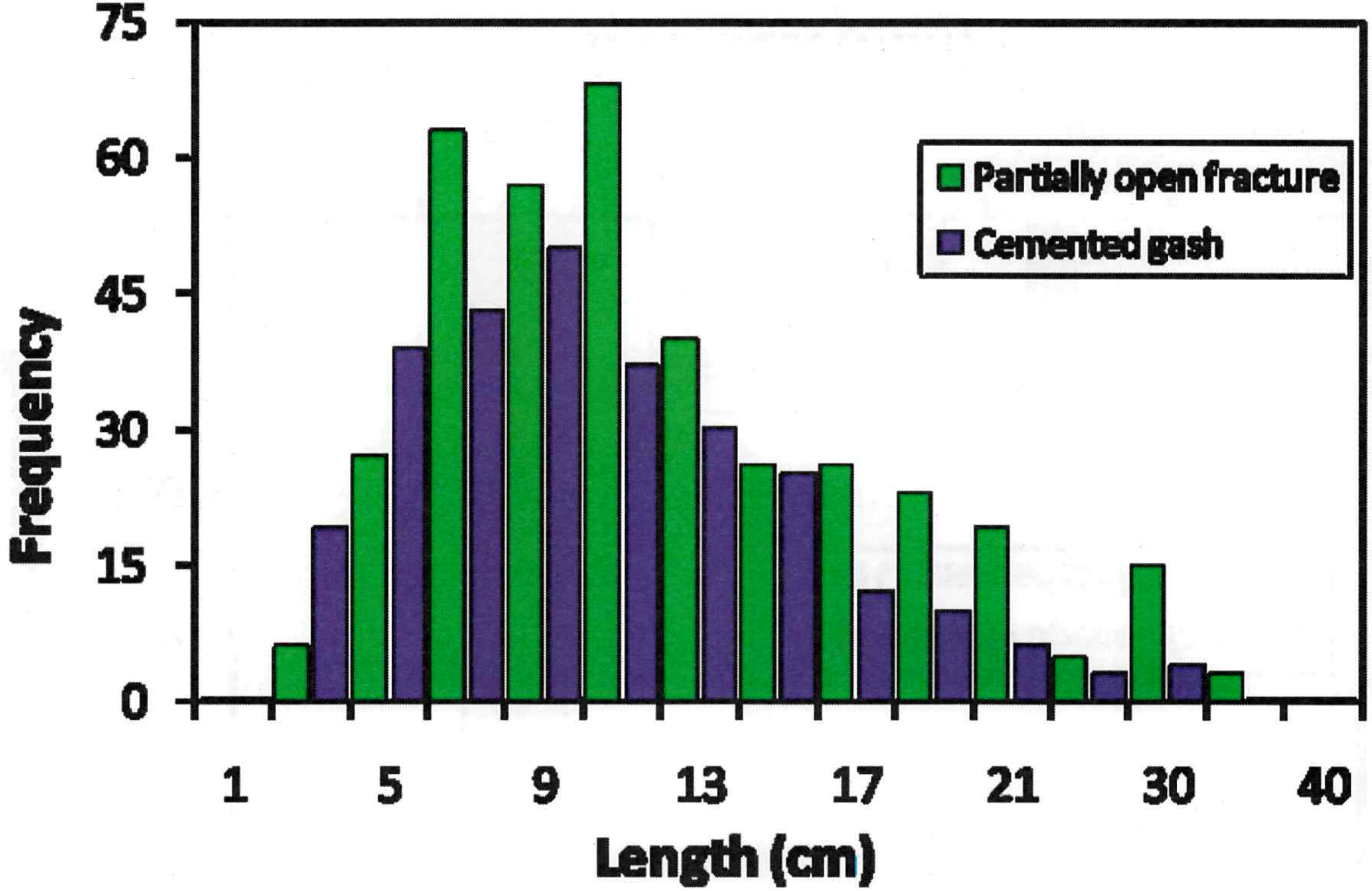
75
60
45
30
15
0
Frequency
Partially open fracture
Cemented gash
1
5
9
13
17
21
30
40
Length (cm)

Figure 15
Click here to download high resolution image

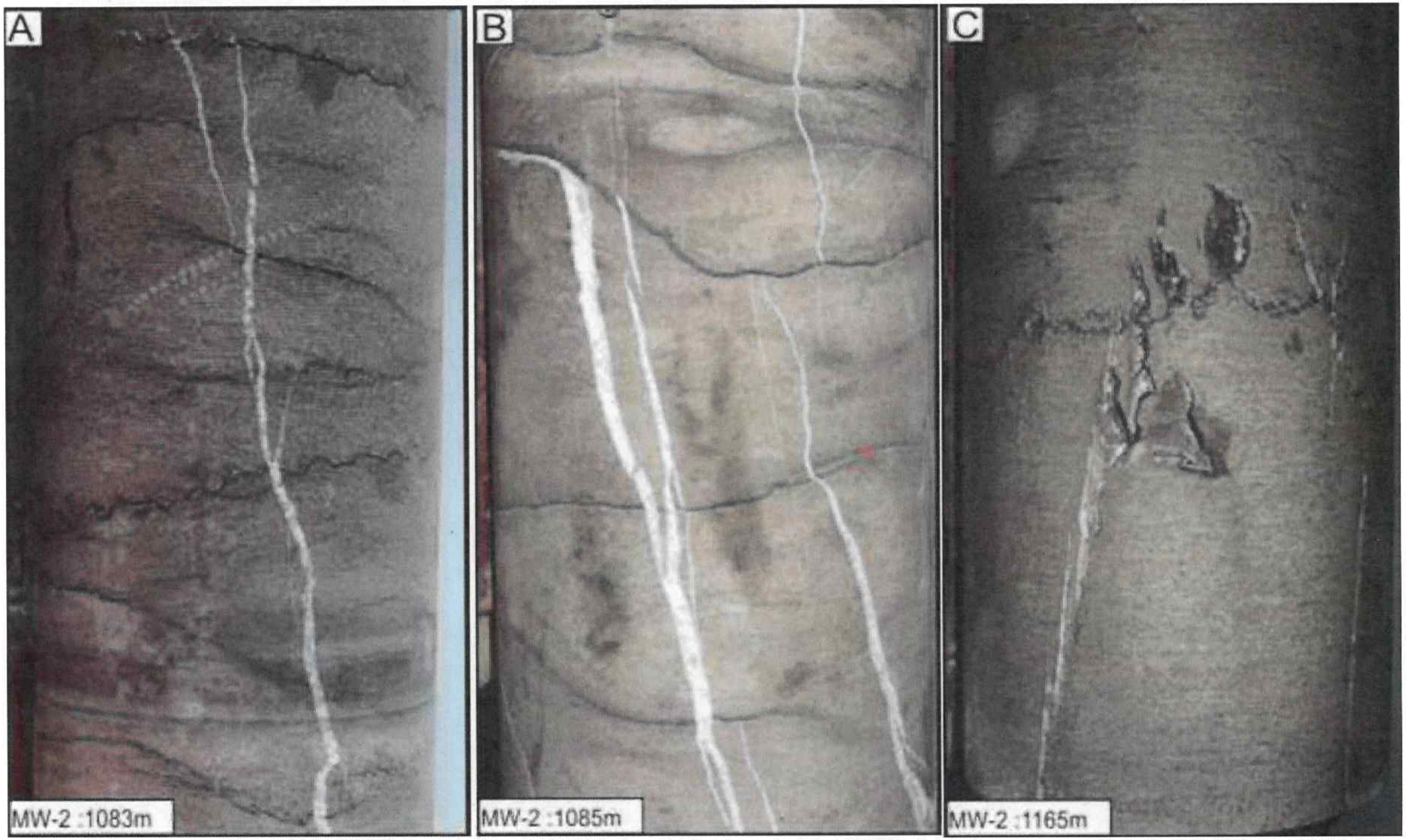

Figure 10
Click here to download high resolution image

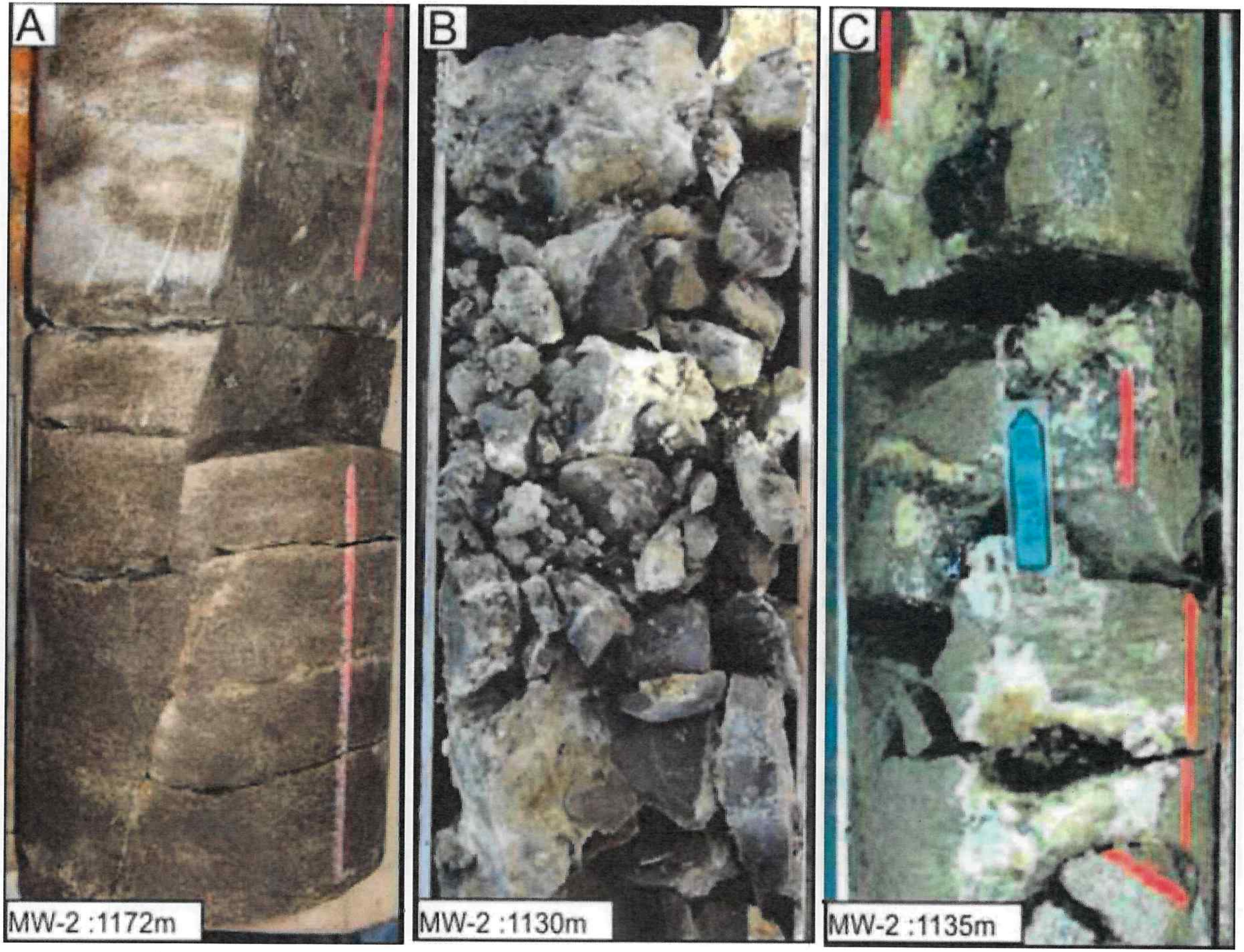

Figure 17

Click here to download high resolution image

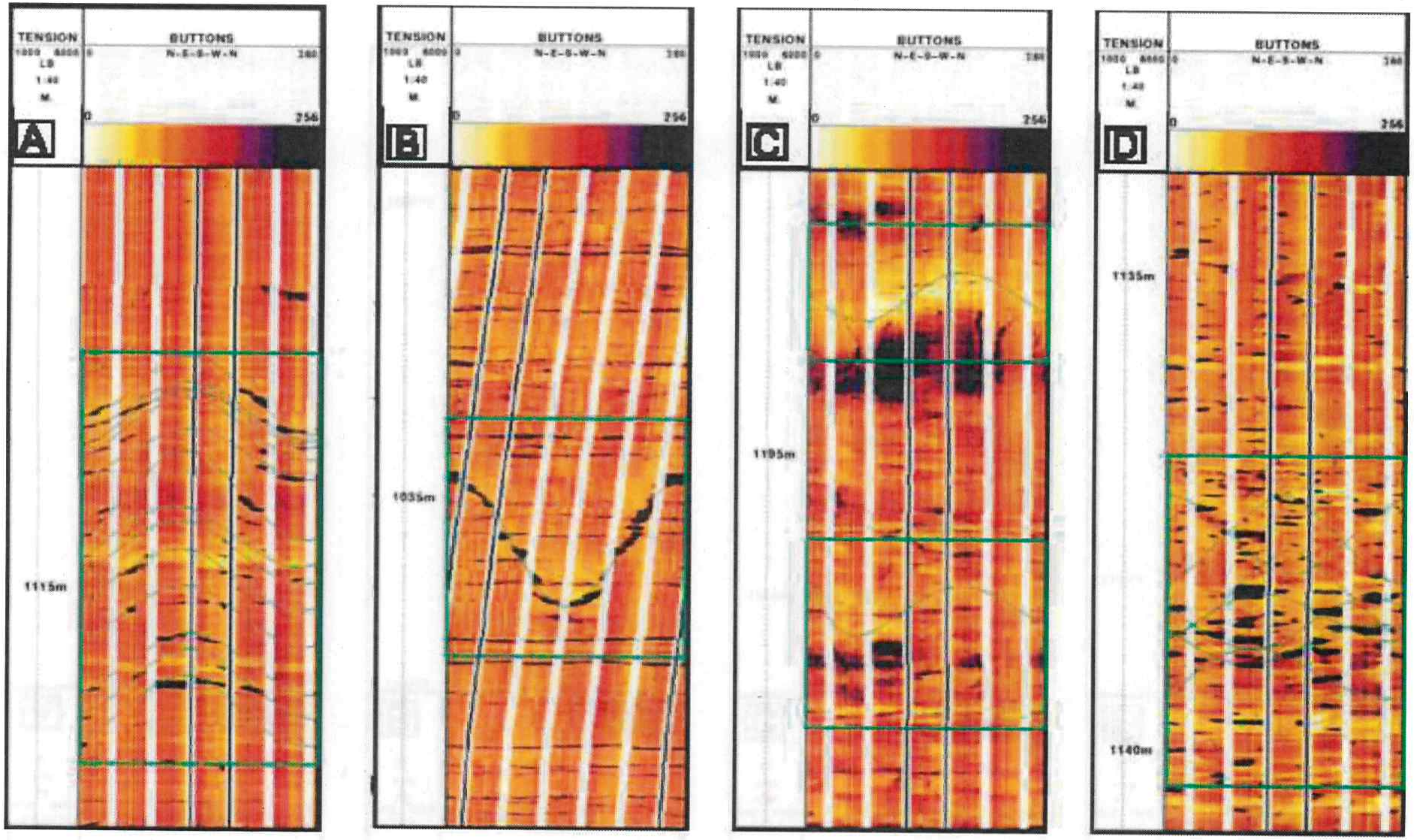

Figure 18
Click here to download high resolution image

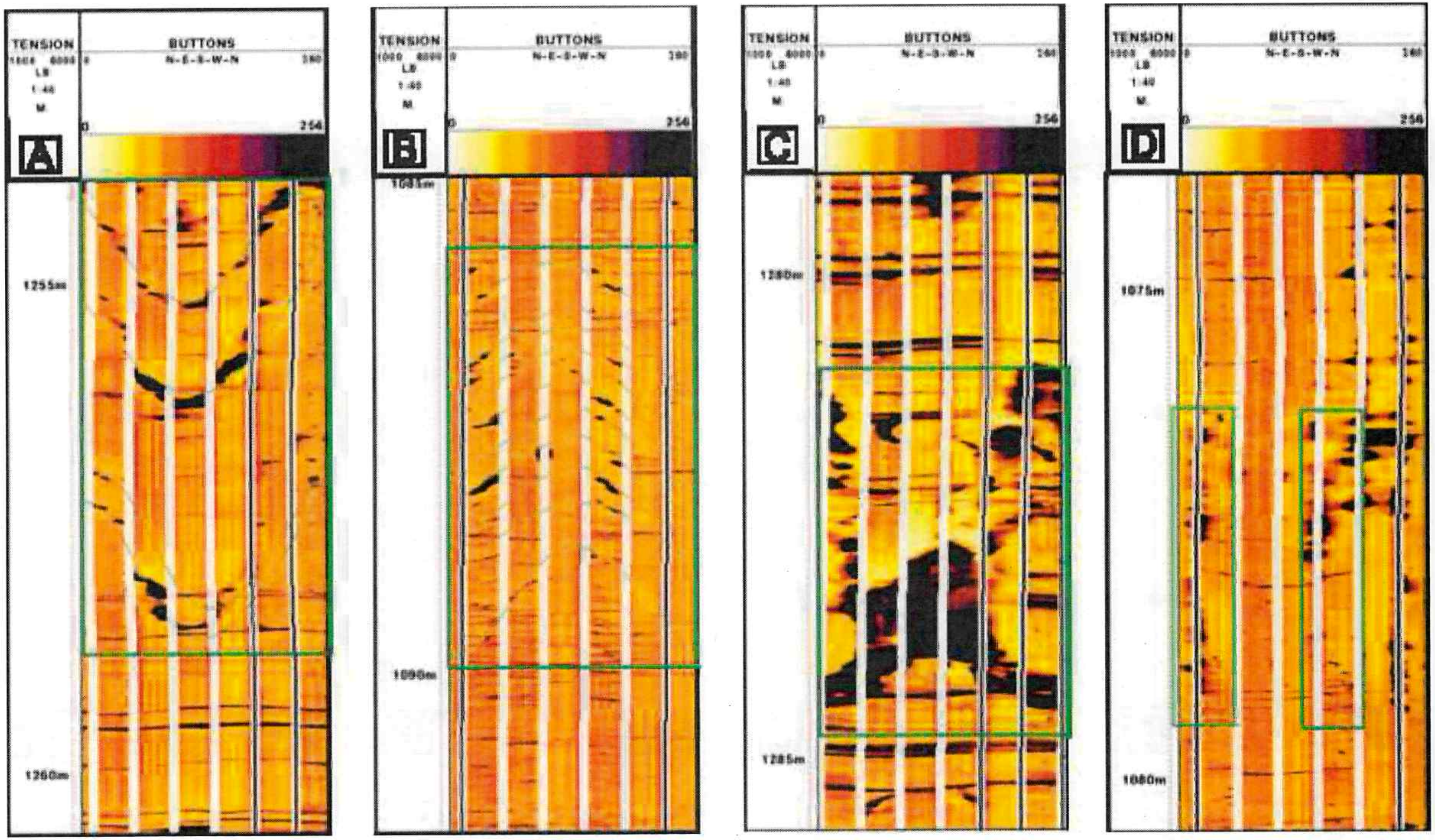

Figure 19
Click here to download high resolution image

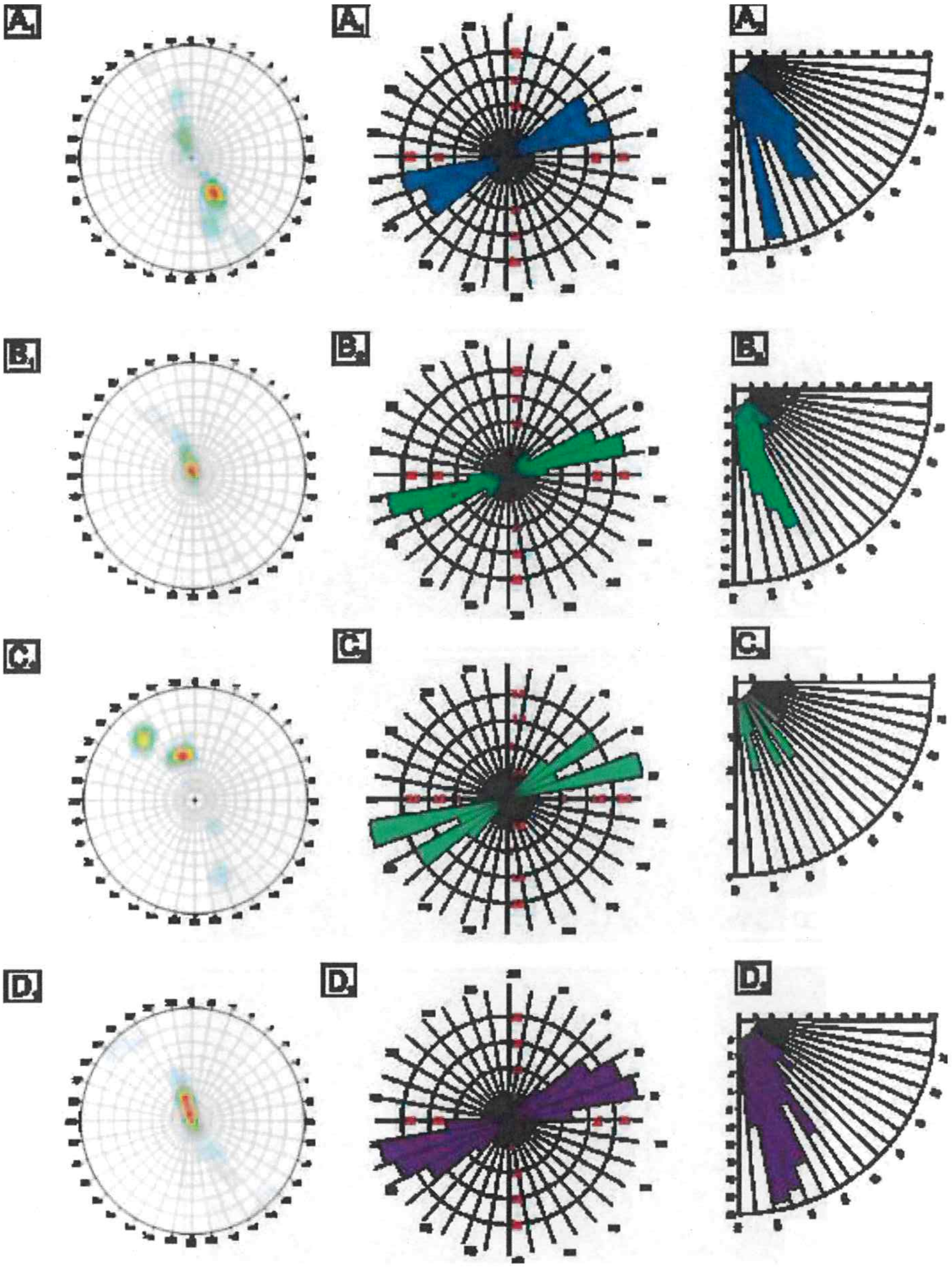

Figure 20
Click here to download high resolution image

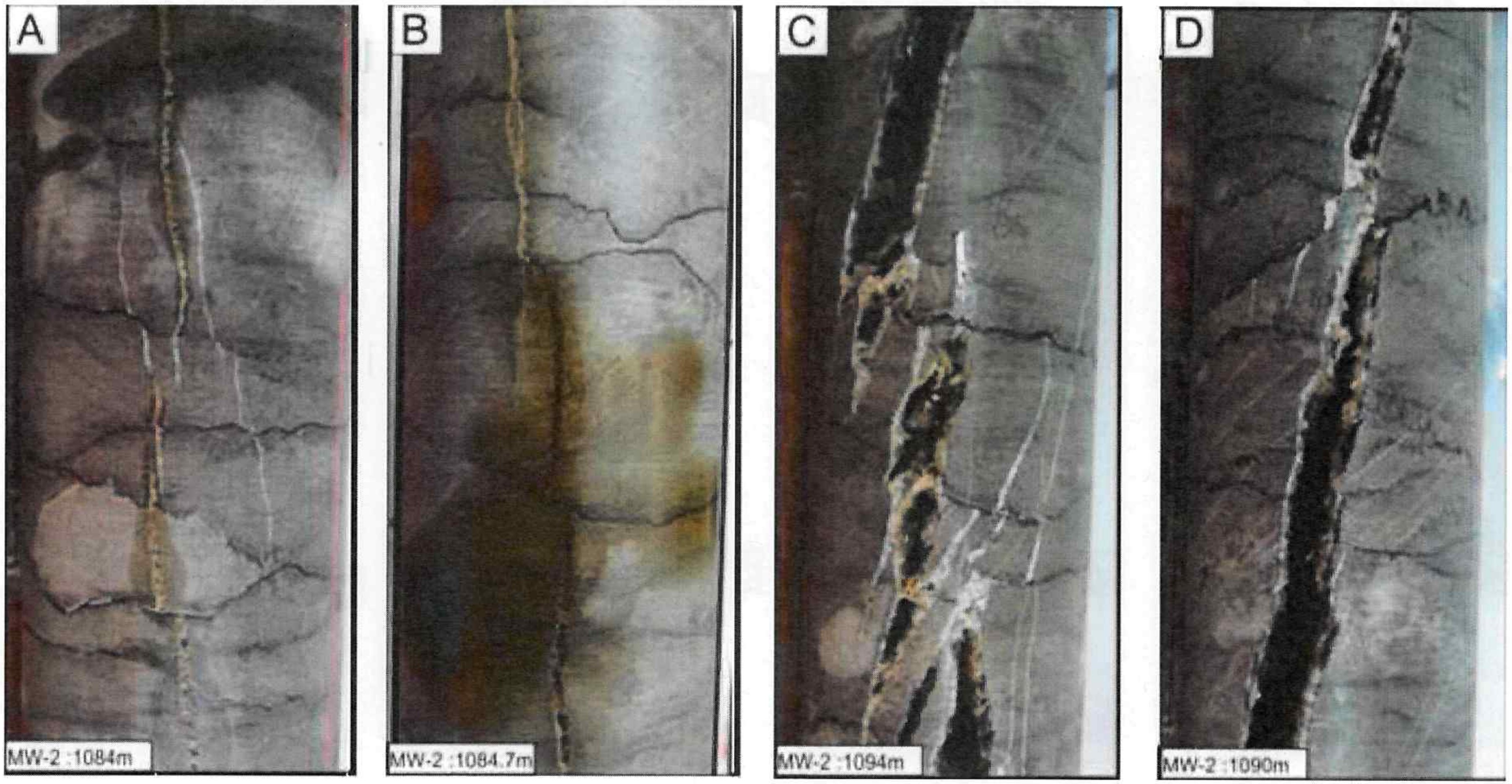

Figure 21

Click here to download high resolution image

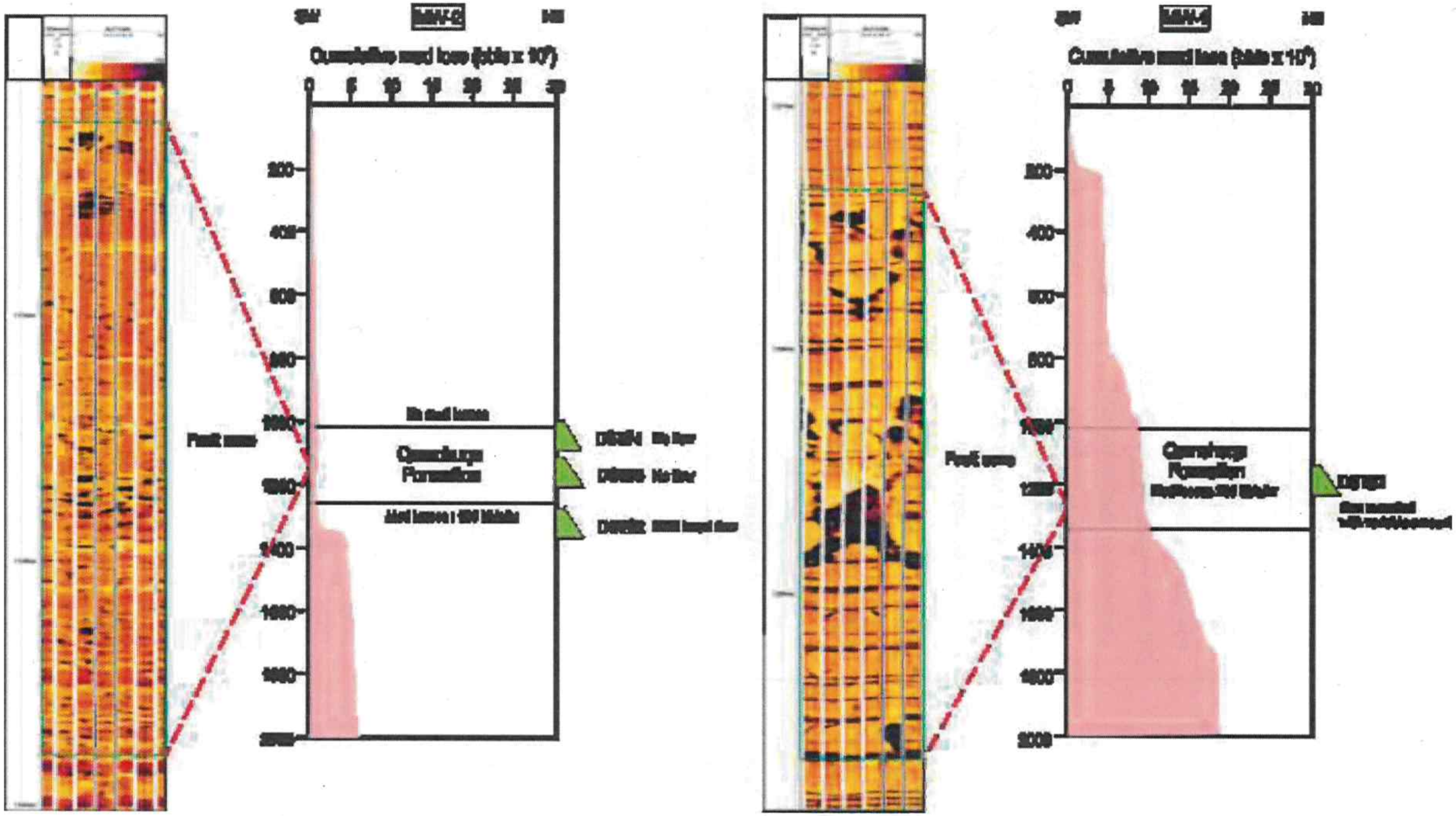

Table 1

Table (1)

Data	MW-1	MW-2
Core	-	102 m
Wireline Log	Gamma ray (GR), Spontaneous Potential (SP), Caliper (CAL), Sonic (DT), Compensated Density Log (CDL), Compensated Neutron Log (CNL), Shallow Laterolog(LLS), Deep Laterolog(LLD) MicroSpherically Focused Log(MSFL), Micro-resistivity Image Log(XRMI)	Gamma ray (GR), Spontaneous Potential (SP), Caliper (CAL), Sonic (DT), Compensated Density Log (CDL), Compensated Neutron Log (CNL), Shallow Laterolog(LLS), Deep Laterolog(LLD) MicroSpherically Focused Log(MSFL), Micro-resistivity Image Log(XRMI)
Cutting sample	200	250
Well Test	Drill Stem Test (DST) 5, Repeat Formation Test (RFT)	Drill Stem Test (DST) 3 and 4 , Repeat Formation Test (RFT)
Mud Log	Mud losses report	Mud losses report

Table 2

Table (2)

Fracture type	Term	XRMI-image feature
Open fracture	Electrically conductive feature	Electrical features crossing the borehole continuously, producing complete sine waves on the micro-resistivity Image logs. They have a clear conductive nature, expecting they are open, and Planar to sub-planar.
Partially open fracture	Partially electrically conductive	Abrupt electrical feature a cross the bore hole on the micro-resistivity image logs. They are irregular to sub-planer and they have only a portion conductive nature.
Closed or filled fracture	Electrically resistive feature	Electrical features crossing the borehole continuously, producing complete sine waves on the micro-resistivity Image logs. They have a resistive nature behavior. They are cemented and usually planar to sub-planar.
Open fracture	Low confidence electrically conductive features	Weak conductive nature can be seen a cross the bore hole on the micro-resistivity image log. They are slightly open fractures or contain conductive material.
Closed or filled fracture	Low confidence electrically resistive features	Weak resistive nature visible a cross the bore hole on the micro-resistivity image log. They are cemented, and occasionally cannot be seen clearly if the rock matrix and cement have similar composition.
Fault	Resistivity contrast	Large, wide and distinct conductive features and high resistivity characters can be seen on micro-resistivity image logs a cross bore hole.
Induced fracture	Electrically conductive feature	Vertical to sub-vertical electrical conductive signatures, creating complete sine waves on the micro-resistivity image logs.

Table 3

Table (3)

Matrix	Porosity (%)	Permeability (mD)
Minimum	2.0	0.06
Maximum	21.1	56.4
Average	10.0	7.65
Fracture	**Porosity (%)**	**Permeability (mD)**
Minimum	0.006	1.22
Maximum	1.217	1×10^{8}
Average	0.173	1.8×10^{6}